

Automatic Classical and Quantum Rebound Attacks on AES-like Hashing by Exploiting Related-key Differentials*

Xiaoyang Dong¹, Zhiyu Zhang^{3,4}, Siwei Sun^{2,5} ✉, Congming Wei¹
Xiaoyun Wang^{1,6,7}, and Lei Hu^{3,4}

¹ Institute for Advanced Study, BNRist, Tsinghua University, Beijing, China.
{xiaoyangdong,wcm16,xiaoyunwang}@tsinghua.edu.cn

² School of Cryptology, University of Chinese Academy of Sciences, Beijing, China.
siweisun.isaac@gmail.com

³ State Key Laboratory of Information Security, Institute of Information Engineering, Chinese Academy of Sciences, Beijing, China.
{zhangzhiyu,hulei}@iie.ac.cn

⁴ School of Cyber Security, University of Chinese Academy of Sciences, Beijing, China.

⁵ State Key Laboratory of Cryptology, P.O. Box 5159, Beijing 100878, China.

⁶ Key Laboratory of Cryptologic Technology and Information Security, Ministry of Education, Shandong University, China.

⁷ School of Cyber Science and Technology, Shandong University, Qingdao, China

Abstract. Collision attacks on AES-like hashing (hash functions constructed by plugging AES-like ciphers or permutations into the famous PGV modes or their variants) can be reduced to the problem of finding a pair of inputs respecting a differential of the underlying AES-like primitive whose input and output differences are the same. The rebound attack due to Mendel et al. is a powerful tool for achieving this goal, whose quantum version was first considered by Hosoyamada and Sasaki at EUROCRYPT 2020. In this work, we automate the process of searching for the configurations of rebound attacks by taking related-key differentials of the underlying block cipher into account with the MILP-based approach. In the quantum setting, our model guide the search towards characteristics that minimize the resources (e.g., QRAM) and complexities of the resulting rebound attacks. We apply our method to Saturnin-hash, SKINNY, and Whirlpool and improved results are obtained.

Keywords: Quantum computation · Collision attacks · Rebound attacks · Saturnin · SKINNY · Whirlpool · MILP

1 Introduction

A cryptographic hash function is a primitive that maps a binary string of arbitrary length into a short fixed-length digest, enjoying collision resistance, preim-

* The full version of the paper is available at <https://eprint.iacr.org/2021/1119>

age resistance, and second-preimage resistance. One popular approach for building a cryptographic hash function is to plug a secure block cipher into one of the twelve secure PGV modes [46] to build the compression function, and then iterate it with the Merkle-Damgård paradigm [13,41]. In this work, we focus on the collision resistance of hash functions constructed in this way with AES-like ciphers (named as AES-like hashing) in both the classical and quantum setting.

The differential attack plays an important role in analyzing the collision resistance of a hash function H , since a successful collision attack implies a pair of inputs x and x' with nonzero difference $x \oplus x'$ such that the output difference $H(x) \oplus H(x')$ is zero. In the context of AES-like hashing, due to the feed-forward mechanism of the PGV modes, a collision means the identification of a pair of different inputs conforming a differential of the underlying block cipher whose input and output differences are the same. To be more concrete, let us consider the MMO mode (one of the twelve secure PGV modes) shown in Figure 1: $H(x) \oplus H(x') = 0$ implies $(m \oplus E_K(m)) \oplus (m \oplus \Delta \oplus E_K(m \oplus \Delta)) = 0$ or $E_K(m) \oplus E_K(m \oplus \Delta) = \Delta$. Therefore, finding a collision is equivalent to finding a pair conforming a differential of the underlying block cipher whose input and output differences are of the same value. One method for achieving this goal is the rebound attack [39], which is the main technique involved in this work.

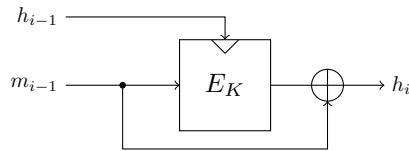


Fig. 1: (MMO) Matyas-Meyer-Oseas

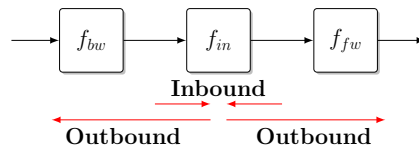


Fig. 2: The Rebound Attack

1.1 The Rebound Attack

The rebound attack was first introduced by Mendel et al. at FSE 2009 [39]. Essentially, it is a technique for generating a pair of inputs fulfilling a differential $\delta \rightarrow \Delta$ for a block cipher. In the rebound attack, the targeted primitive with a truncated differential trail whose input and output differences share a common pattern is divided into three parts as shown in Figure 2. Then, the attacker generates a lot of pairs (named as starting points in the literature) conforming the inbound differential. Finally, the starting points are propagated forward and backward to identify data pairs fulfilling the outbound differentials and the additional constraint that the input and output differences of the whole trail should be equal.

To increase the number of rounds covered by the inbound differential for AES-like ciphers, the super S-box technique was introduced independently by Gilbert et al. [21] and Lamberg et al. [38], where two consecutive AES-like rounds are considered as a whole with several super S-boxes. Later, Sasaki et al.

[48] showed that the memory complexity of the rebound attack can be significantly reduced by exploiting the differential property of non-full-active Super S-boxes. At CRYPTO 2011, Naya-Plasencia further improved the rebound attack by using better algorithms for merging large lists and finding solutions of the underlying differential trail [43]. The rebound attack has become a basic technique for collision attacks [49,30,32,31,40,16] and distinguishing attacks on various hash functions. It even finds applications in the context of DS-MITM attacks [15,14].

The Role of the Key Expansions. In rebound attacks, the generation of the starting points relies on the degrees of freedom from the encryption data path of the underlying block cipher. A natural idea is to utilize the degrees of freedom from the key-schedule algorithm if we do not require the key to be a prefixed value (e.g., the IV). For the sake of simplicity, let us consider the MMO mode with a single message block (see Figure 1). A standard collision message pair (m, m') satisfies $H(IV, m) = H(IV, m')$, where the master key of the underlying block cipher is fixed and thus no degrees of freedom from the key-schedule algorithm can be used. However, for a semi-free-start collision $H(u, m) = H(u, m')$ ($u \neq IV$) or a free-start collision $H(v, m) = H(v, m')$ ($v \neq v'$), the key is allowed to be changed and thus the degrees of freedom from the key-schedule algorithm may be utilized. At ASIACRYPT 2009, Lamberger et al. presented the semi-free-start collision attacks on reduced Whirlpool by exploiting the degrees of freedom from the key schedule algorithm [38]. Since there is no difference in the key material, this type of attack can be modeled with the MILP-based method presented in [26,18]. At ASIACRYPT 2012, Sasaki et al. [49] applied the rebound attack on Whirlpool with an 8-round related-key truncated differential trail and find an 8-round free-start collision attack. To the best of our knowledge, no automatic method is available to find such free-start collisions based on the rebound attack. Finally, we would like to emphasize the importance of free-start collision attacks: The Merkle-Damgård security reduction assumes that any type of collision for the compression function should be intractable for the attacker, including free-start collisions.

1.2 Collision Attacks with Quantum Computing

For a long time, it was believed that quantum computing would have a limited impact on symmetric ciphers due to the quadratic speedup of an exhaustive search attack based on Grover's algorithm [25]. In ISIT 2010, Kuwakado and Morii showed how to break some provable secure schemes in the quantum setting [36], and this naive view started to change. Some follow-up works break more constructions [37,34]. However, a key step in these attacks involving the application of Simon's algorithm on a function with a hidden period related to the secret key, which requires the access to the keyed quantum oracle of the target. This is a strong requirement whose practical relevance is questioned. Hence, quantum attacks with higher complexities are still meaningful if they

do not need to make online queries to superposition oracles of keyed primitives [7,29,35,44,24,28,6].

As keyless primitives, hash functions can be quantumly implemented offline and the thus attackers can freely make quantum superposition queries. For a hash function with n -bit output, classical algorithms find collisions with time complexity $O(2^{n/2})$. In the quantum setting, we have the following bounds induced by generic quantum attacks on hash functions.

- The BHT algorithm [8] equipped with a qRAM with size S finds a collision with a time complexity $T = \frac{2^{n/2}}{\sqrt{S}}$. It achieves optimal tradeoff when $T = 2^{n/3}$ and $S = 2^{n/3}$.
- Since the existence of large qRAM is still doubtful [23,22], there is a time-space tradeoff attack without qRAM, namely the quantum version of parallel rho’s algorithm [50,26,4]. It achieves a time complexity of $T = \frac{2^{n/2}}{S}$ with S processors.
- The CNS algorithm [10] finds a collision with time complexity $T = 2^{2n/5}$ requiring a classical memory of size $2^{n/5}$ and $O(n)$ qubits.

At EUROCRYPT 2020, Hosoyamada and Sasaki [26] introduced the first dedicated quantum attack on hash functions (a quantum version of the rebound attack), which reveals that a differential trail whose probability is too low to be used in the classical setting may be exploitable in quantum attacks. However, the presented attacks are inferior to the CNS attack when there is no large qRAMs. At ASIACRYPT 2020, Dong et al. [18] reduced or even avoid the use of qRAM in the quantum rebound attacks by leveraging the non-full-active Super S-box technique. Recently, Hosoyamada and Sasaki [27] converted the classical semi-free-start collision attack on reduced SHA-2 into quantum collision attack and significantly improved the number of rounds attacked. At ToSC 2021, Chauhan et al. [11] found quantum collisions on reduced AES-256 in double block length hashing. Ni et al. [45] investigated the quantum collision attacks on reduced `Simpira v2` in hashing modes.

1.3 Our Contribution

In this paper, we introduce an automatic tool to determine the related-key differentials, which are optimized for rebound attacks. More concretely, we focus on the free-start collision attacks based on rebound attack technique.

The main task is to increase the probability of the differential trail of the outbound part by properly consuming the degrees of freedom of the key. In addition, we have to deal with the *linear incompatibility*, which are frequently encountered in various automatic tools about related-key differential on AES-like ciphers, such as [5,20,12]. At CRYPTO 2013, Fouque et al. [20] find that the difference cancellation between the AES-128’s key state and the round state in some round imposes some linear relationship between the key and state differences. Hence, difference cancellation in a different round cannot be independently simulated.

On ciphers with linear key schedule, Cid et al. [12] described an MILP model to search the related-key differentials, i.e., **Deoxys-BC** [33]. Since the relationship between **Deoxys-BC**'s round keys are somewhat weakened by the LFSRs, they do not need to consider incompatibilities between many rounds. In this paper, we study a more complex case, i.e., **Saturnin** [9], a round 2 candidate of NIST LWC competition, proposed by Canteaut et al. In **Saturnin**, the round keys are identical for the even or odd rounds, respectively, and the round key in the odd rounds are derived by shifting the key in even round by 5 cells. Hence, the relationships between the round keys in **Saturnin** are stronger, and Cid et al.'s model may lead to many incompatible solutions for **Saturnin**. To deal with the problem, we build an efficient method to fast abandon the incompatible solutions, where the incompatibilities come from many rounds, for example, contradictions between the truncated differentials in round 0 and round 6. In addition, we also model the inbound phase with key differences, where both the 2-round and 3-round inbound phases are considered. We build a uniform objective function on the time complexity to perform the rebound attack, that takes the complexity of solving the inbound phase and the probability of the outbound phase as a whole. Thereafter, we find an 8-round trail for the rebound attacks and generate an 8-round quantum free-start collision attack on the compression function of **Saturnin-hash**. In addition, we also identify a 7-round quantum collision attack on **Saturnin-hash** based on a 7-round single-key rebound attack trail.

We also apply the automatic model to **SKINNY-128-384** [3]. Since **SKINNY** adopts non-MDS matrix, we build a dedicated method to solve the super S-box with non-MDS matrix. Compared to the usual super S-box with MDS matrix, our method explores the details of the non-MDS matrix of **SKINNY** and decomposes the super S-box into a sequence of small S-boxes. Our super S-box technique with non-MDS matrix does not need to precompute the differential distribution of the super S-box even in the full active case, which works efficiently in quantum attack without qRAM and large classic memory. Concretely, about $\sqrt{2^c}$ time is needed to solve the full active super S-box with non-MDS matrix quantumly without qRAM, while the time is $\sqrt{2^{dc}}$ for full active super S-box with MDS matrix, where $d = 4$ for **SKINNY** and **AES**. Thereafter, we give the 16-round free-start quantum collision attacks on the hashing modes with **SKINNY-128-384**.

On ciphers with nonlinear key schedule, we study the compression function of ISO standard hash function, **Whirlpool** [2]. In the automatic model, we place the 3-round inbound phase in both the key schedule path and data encryption path (we do not find better trail with the two-round inbound phases). In its quantum attack, we nest mutiple Grover's algorithms to solve several local searching problems. For **Saturnin**, the role of the consumption of degrees of freedom for key schedule is mainly to increase the probability of the outbound phase of the encryption data path. However, for **Whirlpool**, we have to consume the degrees of freedom of the key to increase the probabilities of the outbound phases in both the key schedule and the encryption data path. Finally, we introduce a 9-round quantum free-start collision attack on the compression function

of `Whirlpool`, while the best previous attack is 8-round in classical setting [49]. The results are summarized in Table 1. Our quantum attacks do not need qRAM or classical memories, which perform better than the generic quantum collision attacks by parallel rho’s algorithm [50,26,4]. However, certain time complexities may be inferior to the quantum attacks equipped with large classical memory by Chailloux, Naya-Plasencia, and Schrottenloher’s algorithm [10].

Table 1: A Summary of the results.

Whirlpool							
Target	Attack	Rounds	Time	C-Mem	qRAM	Setting	Ref.
Hash function	Collision	4/10	2^{120}	2^{16}	-	Classic	[39]
		5/10	2^{120}	2^{64}	-	Classic	[21,38]
		6/10	2^{228}	-	-	Quantum	[26]
		6/10	2^{248}	2^{248}	-	Classic	[17]
	Preimage	5/10	2^{504}	2^8	-	-	[47]
		6/10	2^{481}	2^{256}	-	Classic	[49]
		7/10	2^{497}	2^{128}	-	-	[1]
Compression function	Semi-free-start	5/10	2^{120}	2^{16}	-	Classic	[39]
	Semi-free-start	7/10	2^{184}	2^8	-	Classic	[38]
	free-start	8/10	2^{120}	2^8	-	Classic	[49]
	free-start	9/10	$2^{220.5}$	-	-	Quantum	Sect. 6
	any	any	2^{256}	-	-	Quantum	[50,26,4]
	any	any	$2^{170.7}$	-	$2^{170.7}$	Quantum	[8]
	any	any	$2^{204.8}$	$2^{102.4}$	-	Quantum	[10]
Saturnin-hash							
Hash	Collision	5/16	2^{64}	2^{66}	-	Classic	Full Ver. [19]
		7/16	$2^{113.5}$	-	-	Quantum	Full Ver. [19]
	Preimage	7/16	2^{232}	2^{48}	-	Classic	[17]
Compression function	Free-start	6/16	2^{80}	2^{66}	-	Classic	Full Ver. [19]
	Semi-free	7/16	$2^{90.99}$	-	-	Quantum	Full Ver. [19]
	Free-start	8/16	$2^{122.5}$	-	-	Quantum	Sect. 4
	any	any	2^{128}	-	-	Quantum	[50,26,4]
	any	any	$2^{85.3}$	-	$2^{85.3}$	Quantum	[8]
	any	any	$2^{102.4}$	$2^{51.2}$	-	Quantum	[10]
SKINNY-128-384-MMO/MP							
Compression func.	Free-start	16	$2^{59.8}$	-	-	Quantum	Sect. 5
	any	any	2^{64}	-	-	Quantum	[50,26,4]
	any	any	$2^{42.7}$	-	$2^{42.7}$	Quantum	[8]
	any	any	$2^{51.2}$	$2^{25.6}$	-	Quantum	[10]

2 Preliminaries

2.1 Quantum Computation and Quantum RAM

The state space of an n -qubit quantum system is the set of all unit vectors in \mathbb{C}^{2^n} under the orthonormal basis $\{|0 \cdots 00\rangle, |0 \cdots 01\rangle, \dots, |1 \cdots 11\rangle\}$, alternatively written as $\{|i\rangle : 0 \leq i < 2^n\}$. Quantum computation is achieved by manipulating the state of an n -qubit system by a sequence of unitary transformations and measurements.

Superposition Oracles for Classical Circuit. The superposition oracle of a Boolean function $f : \mathbb{F}_2^n \rightarrow \mathbb{F}_2$ is the unitary transformation \mathcal{U}_f acting on an $(n + 1)$ -qubit system with the following functionality

$$\mathcal{U}_f \left(\sum_{x \in \mathbb{F}_2^n} a_x |x\rangle |y\rangle \right) = \sum_{x \in \mathbb{F}_2^n} a_x |x\rangle |y \oplus f(x)\rangle.$$

Grover's Algorithm. Given a quantum black-box access to a Boolean function $f : \mathbb{F}_2^n \rightarrow \mathbb{F}_2$ with $0 < f^{-1}(1) \ll 2^n$. Grover's algorithm finds an element $x \in \mathbb{F}_2^n$ such that $f(x) = 1$ with $O(\sqrt{2^n/|f^{-1}(1)|})$ calls to the quantum oracle \mathcal{U}_f that outputs $\sum_x a_x |x\rangle |y \oplus f(x)\rangle$ upon input of $\sum_x a_x |x\rangle |y\rangle$. To be more specific, Grover's algorithm iteratively apply the unitary transformation $(2|\psi\rangle\langle\psi| - I)\mathcal{U}_f$ to the uniform superposition $|\psi\rangle = \frac{1}{\sqrt{2^n}} \sum_{x \in \mathbb{F}_2^n} |x\rangle$ of all basis vectors produced by applying the Hadamard transformation $H^{\otimes n}$ to $|0\rangle^{\otimes n}$. During this process, the amplitudes of those values x with $f(x) = 1$ are amplified. Then, a final measurement gives a value x of interest with an overwhelming probability [25].

Quantum Random Access Memories (qRAM). A quantum random access memory (qRAM) uses n -qubit to address any quantum superposition of 2^n memory cells. For a list of classical data $L = \{x_0, \dots, x_{2^n-1}\}$ with $x_i \in \mathbb{F}_2^n$, the qRAM for L is modeled as an unitary transformation $\mathcal{U}_{\text{qRAM}}^L$ such that

$$\mathcal{U}_{\text{qRAM}}^L \left(\sum_i a_i |i\rangle \otimes |y\rangle \right) = \sum_i a_i |i\rangle \otimes |y \oplus x_i\rangle.$$

Currently, it is unknown how a large qRAM can be built. Therefore, quantum algorithms using less or no qRAM are preferred.

2.2 The Full-Active and Non-full-active Super S-box Technique

The super S-box technique proposed by Gilbert et al.[21] and Lamberger et al. [38] extends the Mendel et al.'s [39] inbound part into 2 S-box layers, by identifying four non-interfering $\mathbb{F}_2^{32} \rightarrow \mathbb{F}_2^{32}$ permutations across two consecutive AES rounds and regarding them as four super S-boxes as shown in Figure 3 (a). In [48], Sasaki et al. further reduced the the memory complexity by considering non-full-active super S-boxes as shown in Figure 3 (b).

Full-active super S-box. We consider a more general scenario that the internal state of the cipher is a $d \times d$ matrix of c -bit cells. As shown in Figure 3 (a) with $d = 4$, for the i th super S-box SSB_i and given input difference $\Delta X_1^{(i)}$, we compute $\Delta Y_2^{(i)} = \text{SSB}_i(x \oplus \Delta X_1^{(i)}) \oplus \text{SSB}_i(x)$ for $x \in \mathbb{F}_2^{dc}$. Store the pair $(x, x \oplus \Delta X_1^{(i)})$ in a table $\mathbb{L}^{(i)}[\Delta Y_2^{(i)}]$. In the inbound phase, given $\Delta_{in} = \Delta Z_0$, we compute $\Delta X_1^{(i)}$ for $0 \leq i \leq d - 1$, then we compute the d tables $\mathbb{L}^{(0)}, \mathbb{L}^{(1)}, \dots, \mathbb{L}^{(d-1)}$.

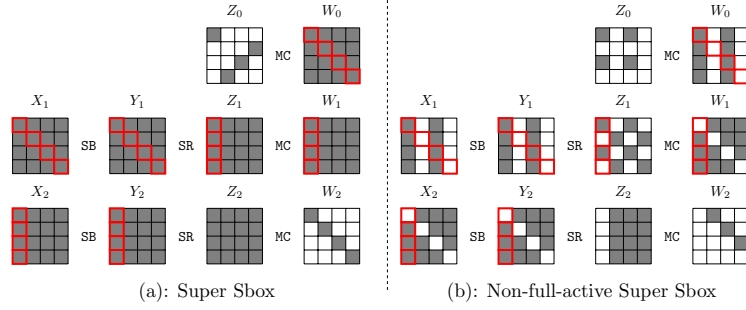


Fig. 3: A differential with non-full-active super S-box

For each $\Delta_{out} = \Delta W_2 \in \mathbb{F}_2^{dc}$, compute $\Delta Y_2^{(i)}$ with $0 \leq i \leq d-1$ to access the table $\mathbb{L}^{(i)}[\Delta Y_2^{(i)}]$ to generate a pair conforming the truncated differential of the inbound part. Hence, for given Δ_{in} , we need $d \times 2^{dc}$ memory to store the four tables, and will generate $|\Delta_{out}| = 2^{dc}$ pairs on average satisfying the inbound part.

At EUROCRYPT 2020, Hosoyamada and Sasaki [26] converted the classical super S-box technique into a quantum one. They introduced two quantum ways. The first one is to use the qRAM to replace the classical memory to store the super S-box, which needs an exponential size of qRAM. The second one is to apply the Grover's algorithm to search a conforming pair for a given input-output difference $(\Delta X_1^{(i)}, \Delta Y_2^{(i)})$ of SSB_i . This method needs about $2^{dc/2}$ super S-box computations to find the right pair.

Non-full-active super S-box. For the non-full-active super S-box in Figure 3 (b), the Property 1 of MDS in MC is used. Look at $\Delta W_1 = \text{MC}(\Delta Z_1)$, suppose there are totally s non-active cells ($s < d$) and $2d - s$ active cells in ΔZ_1 and ΔW_1 ($s = 3$ in Figure 3 (b)), then by guessing the differences of $d - s$ active cells, we can determine other differences according to Property 1. Then, for a fixed input-output differences $(\Delta X_1^{(i)}, \Delta Y_2^{(i)})$ of SSB_i , we can deduce all the input-output differences for the $2d - s$ active cells of two S-box layers for each guess and then deduce their values by accessing the differential distribution table (DDT) of the S-box. Now, for the equation $W_1 = \text{MC}(Z_1)$, we have $2d - s$ known cells in W_1 and Z_1 , hence it acts of probability $2^{-(2d-s-d)c} = 2^{(s-d)c}$. Hence, for a fixed $(\Delta X_1^{(i)}, \Delta Y_2^{(i)})$, we get $2^{(d-s)c} \cdot 2^{(s-d)c} = 1$ conforming pair on average. The time complexity is $2^{(d-s)c}$. The memory is 2^{2c} to store the DDT of S-box.

Property 1. $\text{MC} \cdot (Z[1], Z[2], \dots, Z[d])^T = (W[1], W[2], \dots, W[d])^T$ can be used to fully determine the remaining unknowns if any d cells of Z, W are known.

In the quantum setting, Dong et al. [18] converted the non-full-active super S-box technique into a quantum one by searching the $2^{(d-s)c}$ differences with Grover's algorithm, which gains a square root speedup. Both in quantum and classical setting, the complexity is determined by the number of inactive cells in $(\Delta X_1^{(i)}, \Delta Y_2^{(i)})$, i.e., s .

2.3 Inbound Part with Three Full Rounds

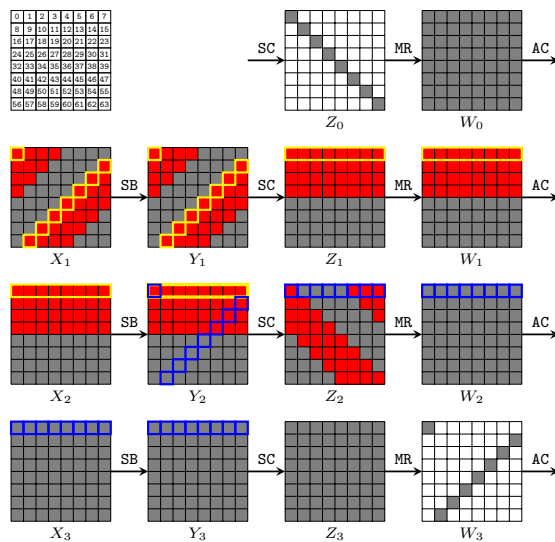


Fig. 4: Details in inbound phase covering 3 rounds

As shown in Figure 4, given fixed differences ΔZ_0 and ΔW_3 , Jean et al. [30] introduced an algorithm to find the pairs of conforming to the 3-round differential. At EUROCRYPT 2020, Hosoyamada and Sasaki [26] introduced a memoryless algorithm (see Algorithm 9 of our full version paper). The time complexity is $2^{d^2c/2+dc}$ and there expects one conforming pair. Hosoyamada and Sasaki [26] also introduced the quantum variant shown in Section 6.

3 Modeling Rebound Attacks in the Related-key Setting

In the related-key setting, taken MMO mode as an example in Figure 1, we construct free-start collisions using related-key truncated differential trail of E_K , which meets Equation (1):

$$(m \oplus E_K(m)) \oplus (m \oplus \Delta m \oplus E_{K \oplus \Delta K}(m \oplus \Delta m)) = \Delta m \oplus \Delta m = 0. \quad (1)$$

The procedures of the related-key rebound attack are:

1. Find a related-key truncated differential for E_K ,
2. Choose a key pair (K, K') which meets the differential in the key-schedule,
3. Perform the rebound attack in the encryption data path with (K, K') .

The Outbound Phase. In the single-key setting, previous works [26,18] consider the probability of the truncated differential, which is mainly due to the

cancellations of MC operation. In the related-key setting, we try to use similar method directly, i.e., calculating the probability of differential transition by counting the number of inactive cells in the output of linear operations (e.g. MC, AK etc.) whose input is active. We use the round function of AES as an example without the SR. In Figure 5(a), the four cells in first column of Y_i are active which are the input to the MC operation. The first column of Z_i has one inactive cell. Assume the differences in all active cells are independent uniform random, then $Prob(Y_i \rightarrow Z_i) \approx 2^{-c}$ (one cell of the state is of c bits). Similarly, $Prob(Z_i \rightarrow W_i) \approx 2^{-c}$. Thus the probability of the truncated differential trail in Figure 5(a) is about 2^{-2c} .

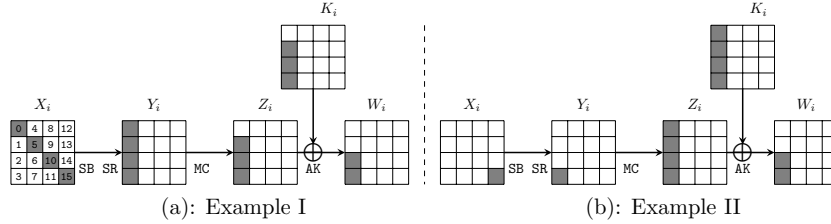


Fig. 5: AES rounds in forward outbound phase.

The method borrowed from single-key rebound attack seems to work well, but in related-key setting, this method may lead to a lower probability than the reality. For example, in Figure 5(b), two active cells are cancelled by AK operation. Using the above method, we can calculate the probability of the trail is about 2^{-2c} . Note that in the related-key rebound attack, the key pair is first determined, then perform the rebound attack in the encryption data path, where key materials act as constants. Hence, the probability of the outbound phase in the encryption data path is computed under a fixed key difference. Therefore, $\Delta K_i[0, 1] = \Delta Z_i[0, 1]$ and $\Delta Z_i[0, 1]$ is fixed. Due to Property 1, all other active cells of differences in Y_i and Z_i are determined. Hence, the probability of the differential is determined by the differential propagation of the S-box, i.e., $Prob(\Delta X_i[15] \xrightarrow{S\text{-box}} \Delta Y_i[3]) > 2^{-c}$ with DDT, which is bigger than 2^{-2c} . In detail, we derive the relationship between the first column of Y_i and Z_i from MC as shown in Equation (2).

$$\begin{bmatrix} \Delta Z_i[0] \\ \Delta Z_i[1] \\ \Delta Z_i[2] \\ \Delta Z_i[3] \end{bmatrix} = \begin{bmatrix} 02 & 03 & 01 & 01 \\ 01 & 02 & 03 & 01 \\ 01 & 01 & 02 & 03 \\ 03 & 01 & 01 & 02 \end{bmatrix} \times \begin{bmatrix} \Delta Y_i[0] \\ \Delta Y_i[1] \\ \Delta Y_i[2] \\ \Delta Y_i[3] \end{bmatrix}. \quad (2)$$

As 3 cells in the 1st column of ΔY_i are 0 and $\Delta Z_i[0, 1] = \Delta K_i[0, 1]$, we have

$$\begin{bmatrix} \Delta K_i[0] \\ \Delta K_i[1] \\ \Delta Z_i[2] \\ \Delta Z_i[3] \end{bmatrix} = \begin{bmatrix} 02 & 03 & 01 & 01 \\ 01 & 02 & 03 & 01 \\ 01 & 01 & 02 & 03 \\ 03 & 01 & 01 & 02 \end{bmatrix} \times \begin{bmatrix} 0 \\ 0 \\ 0 \\ \Delta Y_i[3] \end{bmatrix},$$

which shows that $\Delta Y_i[3] = \Delta K_i[0] = \Delta K_i[1]$. Hence, $\Delta K_i[0]$ and $\Delta K_i[1]$ are related to each other. We call the number of cells in key, whose differences can be chosen independent randomly, the *degree of freedom* in the key differential states. In Figure 5(b), key states have four active cells, among them two cells meet the condition $\Delta K_i[0] = \Delta K_i[1]$ that consumes one-cell degree of freedom. Hence, the degrees of freedom in the key differential states are $4-1=3$ in Figure 5(b). Therefore, the degree of freedom in K is reduced to increase the probability of the trail in Figure 5(b) from 2^{-2c} to about 2^{-c} . The consumption of freedom in the whole differential trail should not be higher than the number of active cells in key. Note that similar technique has already been used by Cid et al. [12] in the cryptanalysis of Deoxys against related-key differential attack. We apply the technique to the rebound attack by taking the features of rebound attack into the model.

Degree of Freedom. For a target with linear key schedule algorithms (e.g. *Saturnin* [9] and *SKINNY* [3]), we formulate its degree of freedom in the following. Taking *Saturnin* as an example, if there are t active cells in the master key, then we say that the initial degree of freedom for the key difference is t -cell (denoted by $\text{DoK}=t$), since there are about $(2^c)^t$ different choices for the key difference. However, as discussed previously, in rebound attacks exploiting related-key differentials, we may constrain the key difference by a system of linear equations with the active cells in the master key as variables to increase the probability of the outbound differentials. Assuming we have l independent linear equations, then l -cell degree of freedom is consumed (denoted by $\text{DoK}^- = l$). Therefore, to ensure there is at least one solution for the master key difference, we require $\text{DoK} \geq \text{DoK}^-$. Otherwise, we have an over-defined system of equations for the active cells of the master key, which may have some conflicts.

Besides the degree of freedom from the master key difference, another source of degree of freedom should be considered. For a given master key difference, we can form $(2^c)^{\bar{n}}$ key pairs satisfying the given difference, where the key is of \bar{n} c -bit cells. Taking the encryption data path into account and supposing that for a given $(\Delta_{in}, \Delta_{out})$ and key pair (K, K') , there is one solution for the inbound part in the data encryption path on average, then we can generate $(2^c)^{\text{DoK}-\text{DoK}^-+\bar{n}}(|\Delta_{in}| \cdot |\Delta_{out}|)$ starting points as $(K, M, K'M')$, which is called the degrees of freedom for the rebound attack [39] (denoted by DoA). To expect one solution fulfilling the outbound differential with probability p , we require that $(2^c)^{\text{DoA}} = (2^c)^{\text{DoK}-\text{DoK}^-+\bar{n}}(|\Delta_{in}| \cdot |\Delta_{out}|) \geq \frac{1}{p}$.

3.1 Dedicated Modelings and Case Study on Saturnin-hash

Saturnin is a suite of lightweight symmetric algorithms proposed by Canteaut et al. [9]. It is among the 2nd round candidates of the NIST LWC. Based on a 256-bit AES-like block cipher with 256-bit key, two authenticated ciphers and a hash function are designed. In this section, we focus on its hash function, called *Saturnin-Hash*. The round function only consists of *AK*, *SB* layer and linear layer, where *MixRows* (MR) and *MixColumns* (MC) are applied alternatively in

even or odd number of round. The key schedule is linear and simple. In even round, K is used and in odd round the K is rotated by 5 cells (denoted as \tilde{K}).

Related-key Truncated Differential Model. For an R -round primitive, we use several binary variables $x_r^{i,j}$ and $y_r^{i,j}$ to represent the state before and after the MR (or MC) operations in the r -th round, where i and j mean that the cell is in i -th row and j -th column. These variables are 1 if and only if the corresponding cell is active. For the key states, we use $K^{i,j}$ and $\tilde{K}^{i,j}$ to represent the rotated key and the master key in the same way.

Without loss of generality, we only consider MR operation now. To model the MR operations (similar constraints are also applied to MC), we use binary variables b_r^i to express MR operations are active or not in the i -th row of r -th round, and use branch number to generate constraints just like Mouha et al.'s model [42].

Another operation is key addition. The constraint of key addition are quite like constraint of XOR, except the result of two active cells addition can be active or inactive.

The Outbound Phase. As shown in Figure 5(b), the number of cancelled cells could not show the real probability in a related-key model. Hence, the constraints in our model are different from single-key models. We use $Prob_r^i$ to represent the probability of the i -th row in round r .

In forward part of the outbound phase, we use c_r^i to represent the number of cells cancelled after the r -th round MR operation in row i , and \tilde{c}_r^i to represent the number of cells cancelled after the next key addition operation in row i . If $\sum_{j=0}^{j \leq 3} x_r^{i,j} \geq c_r^i + \tilde{c}_r^i$ (like the trail in Figure 5(a)), then the probability of this MR operation in this row is estimated by $c_r^i + \tilde{c}_r^i$ (to show the connection of probabilities and variables in our MILP model, the probabilities are taken in $-\log_{2e}$). If $\sum_{j=0}^{j \leq 3} x_r^{i,j} < c_r^i + \tilde{c}_r^i$ (like the trail in Figure 5(b)), then the probability is $\sum_{j=0}^{j \leq 3} x_r^{i,j}$, and the degree of freedom in key states is consumed $c_r^i + \tilde{c}_r^i - \sum_{j=0}^{j \leq 3} x_r^{i,j}$. Thus, $Prob_r^i = \min(c_r^i + \tilde{c}_r^i, \sum_{j=0}^{j \leq 3} x_r^{i,j})$.

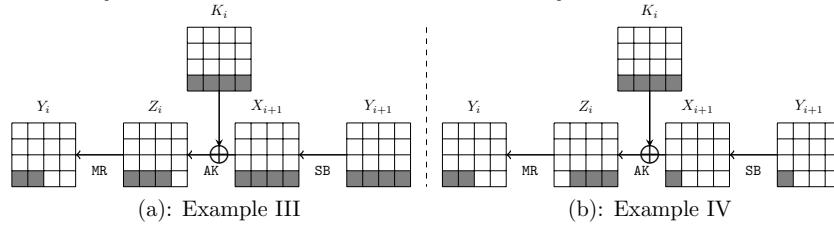


Fig. 6: Saturnin rounds in backward outbound phase.

Similar to forward part, in backward part, we also use c_r^i to represent the number of cells that are cancelled by the r -th round MR^{-1} operation in row i , and \tilde{c}_r^i to represent the number of cells are cancelled before the next key addition operation in row i . If $\sum_{j=0}^{j \leq 3} x_{r+1}^{i,j} \geq c_r^i$ (like the trail in Figure 6(a)), then the probability of this MR operation in this row is $c_r^i + \tilde{c}_r^i$. If $\sum_{j=0}^{j \leq 3} x_{r+1}^{i,j} < c_r^i$ (like the trail in Figure 6(b)), then the cancellation of this MR operation in this row is

$\sum_{j=0}^{j \leq 3} x_{r+1}^{i,j}$, and the degree of freedom in key states is consumed $c_r^i - \sum_{j=0}^{j \leq 3} x_r^{i,j}$. Thus, $Prob_r^i = \min(c_r^i + \tilde{c}_r^i, \sum_{j=0}^{j \leq 3} x_{r+1}^{i,j})$.

To limit the consumption of freedom, we add the following constraint

$$\sum_{Forward} (c_r^i + \tilde{c}_r^i - Prob_r^i) + \sum_{Backward} (c_r^i - Prob_r^i) \leq \sum_{0 \leq i, j \leq 3} K^{i,j}.$$

The Inbound Phase. We use a variable l to determine the inbound part and outbound part, and the inbound part includes r_{in} rounds. Thus round $l + 1$ to $l + r_{in}$ are inbound part, while other rounds are outbound parts. If $r_{in} = 2$, we use the super S-box techniques to solve the inbound part. In classical setting, it usually does not increase the overall time complexity, and only need some memories as shown in Section 2.2. However, in quantum setting without qRAM, the overall time complexity is also affected by the super S-box technique. As shown by Dong et al. [18], if the super S-boxes are not fully active, the time for quantum attack may be reduced. Following the notations in Section 2.2, the number of inactive S-boxes in the i -th super S-box SSB_i is denoted as s^i . Then the quantum time to solve the inbound part is about $\sqrt{2^{d - \min\{s^0, s^1, s^2, s^3\}}}$ according to Dong et al. [18], where d is the number of cells in each row, and $d = 4$ for **Saturnin**. In related-key setting, some cells in super S-boxes can be determined by key difference. As we shown in Algorithm 2 of Section 4, cells with known difference play the same role as inactive cells in non-full active super S-boxes technique. Thus s_i denote the number of cells whose difference is fixed before or after the MR or MC operation in the middle of a super S-box.

When $r_{in} = 3$, the inbound phase is solved by the methods of Jean et al. [30] classically or Hosoyamada et al. [26] quantumly. Both the time complexities are fixed and independent to the rebound attack trails as shown in Section 2.3. We will give more details in the attack on **Whirlpool**, whose rebound trail includes a 3-round inbound part in both the key schedule and encryption data path.

Time Complexity and Objective Function. In quantum setting without qRAM, we have two time complexities according to r_{in} :

- ▶ $r_{in} = 2$, the time complexity is about $\sqrt{2^{(\sum Prob_r^i + \sum x_0^{i,j} + d - \min\{s^0, s^1, s^2, s^3\})}}$, where $\sum Prob_r^i$ corresponds to the probability of the truncated difference of the outbound phase, $\sum x_0^{i,j}$ are the number of active cells to be collided for the plaintext and ciphertext, $d - \min\{s^0, s^1, s^2, s^3\}$ corresponds to the time to solve the inbound part. Hence, when $r_{in} = 2$, the objective function is to minimize $\sum Prob_r^i + \sum x_0^{i,j} + d - \min\{s^0, s^1, s^2, s^3\}$.
- ▶ $r_{in} = 3$, the objective function is $\sum Prob_r^i + \sum x_0^{i,j}$.

The Incompatibilities within Many Rounds. Cid et al. [12] described an MILP model to search the related-key differentials on ciphers with linear key schedule, e.g., **Deoxys-BC** [33]. Since the relationship between **Deoxys-BC**'s round keys are somewhat weakened by the LFSRs, they do not need to consider incompatibilities between many rounds. In **Saturnin**, the round keys are identical for many rounds, which lead to strong relationship on the round keys.

Though we limit the consumption of degree of freedom in our MILP model, a trail can be incompatible when the same key cell needs to satisfy two different relationships in different rounds. For example, in Figure 7, from Y_2 to X_3 we have $(\Delta Z_2[2], \Delta k_{11}, \Delta k_{15}, \Delta k_0) = \text{MR}(\Delta Y_2[2], 0, 0, 0)$. From Y_4 to X_5 we have $(\Delta k_7, \Delta k_{11}, \Delta k_{15}, \Delta k_0) = \text{MR}(\Delta Y_4[2], 0, 0, 0)$. The above two linear equations have 6 same cells., Due to Property 1, $\Delta Z_2[2] = \Delta k_7$, then $\Delta X_3[2]$ should be 0, which is a contradiction.

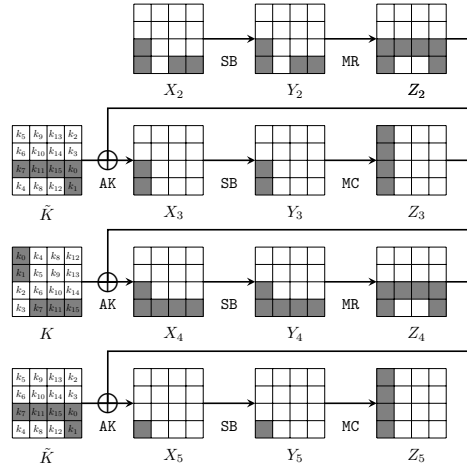


Fig. 7: An incompatible trail of Saturnin

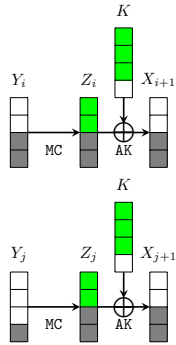


Fig. 8: An incompatible trail

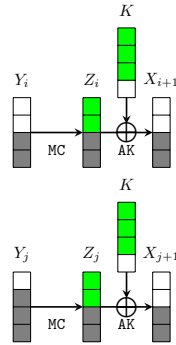


Fig. 9: A compatible trail

Adding more constraints to remove this kind of contradictions in MILP model is quite hard. According to Property 1, a set of equations of MC (or MR) operation has 8 cells of variables, and if two sets of equations have at least 4 same cells, then all cells of variables in the two sets of equations should be same. We use this property to fast delete the incompatible trails. Figure 8 and Figure 9 show

examples of incompatible and compatible trails. The inactive cells are in white and active cells are in gray and green, and the difference in green cells are determined by key difference. We can encode the truncated difference in Y and Z to a 8-dimensional vector $\mathbb{S} = (y_0, y_1, y_2, y_3, z_0, z_1, z_2, z_3)$, where $y_m = 1$ if $\Delta Y[m]$ is inactive with $0 \leq m \leq 3$, else $y_m = 0$; $z_m = 1$ if $\Delta Z[m]$ is 0 or equals to key differences, else $z_m = 0$. For example, in Figure 8, we have $\mathbb{S}_i = (1, 1, 0, 0, 1, 1, 0, 0)$ for round i and $\mathbb{S}_j = (1, 1, 1, 0, 1, 1, 0, 0)$ for round j with the same K . The dot product of two vectors \mathbb{S}_i and \mathbb{S}_j is the number of same cells of two sets of equations of MC (or MR) operations. For example, $\langle \mathbb{S}_i, \mathbb{S}_j \rangle = 4$ in Figure 8, hence, due to Property 1, all the cells of differences in Y_i and Y_j (also for Z_i, Z_j and X_{i+1}, X_{j+1}) should be the same. However, $Y_i[2]$ is active but $Y_j[2]$ is inactive, which leads to contradiction and Figure 8 is an incompatible trail. In Figure 9, we have $\mathbb{S}_i = (1, 1, 0, 0, 1, 1, 0, 0)$ and $\mathbb{S}_j = (1, 0, 0, 0, 1, 1, 0, 0)$ with $\langle \mathbb{S}_i, \mathbb{S}_j \rangle = 3 < 4$, hence the trail is compatible.

Since we can derive the vector \mathbb{S}_i from the solutions of our MILP model, we use the PoolSearchMode of Gurobi to get many solutions for our MILP model and then check if one of the solutions does not have this kind of contradiction. For 8-round **Saturnin** with $l \geq 1$ and $r_{in} = 2$, we get thousands of different truncated differentials from our MILP model through the PoolSearchMode and after checking them with the above method, none of them are left; for 8-round **Saturnin** with $l = 0$ and $r_{in} = 2$, we get a hundred of different truncated differentials and most of them are compatible. For those left solutions, we pick one trail to launch our rebound attacks. See supplementary materials for the source code of constructing MILP model and detecting contradiction. We have put the source code for the automatic model of **Saturnin-hash** in a public domain at <https://github.com/rebound-rk/rebound-rk>

4 Free-Start Collision on 8-round Saturnin-hash

By applying the MILP model, we find an 8-round truncated differential on **Saturnin** as shown in Figure 10(a). We perform the quantum collision attack based on the truncated differential. The inbound phase covers from Y_0 to X_3 , including two SB layers. The two outbound phases are from Y_0 to the plaintext and X_3 to the ciphertext. In the inbound phase, there are four parallel non-full active super S-boxes. The input difference $\Delta_{in} = \Delta X_1$ is determined by ΔY_0 . At round 2 and 3, from $\text{MR}(\Delta Y_2) \oplus \Delta \tilde{K} = \Delta X_3$, at the 3rd row, we get

$$\text{MR}^{-1}(\Delta k_7, \Delta k_{11}, \Delta k_{15}, \Delta k_0) = (\Delta Y_2[2], 0, 0, 0). \quad (3)$$

For row 3 of the computation from ΔY_4 to ΔX_5 , and from ΔY_6 to ΔX_7 , the same requirement of Equation (3) is also applied, since the subkeys are all \tilde{K} and the truncated form are the same.

At round 3 to 4, in the first column of the computation from ΔY_3 to ΔX_4 , we have $\Delta Z_3[0] = \Delta k_0$ and $\Delta Z_3[1] = \Delta k_1$. Further, we get

$$\text{MC}^{-1}(\Delta k_0, \Delta k_1, \Delta Z_3[2], \Delta Z_3[3])^T = (0, 0, 0, \Delta Y_3[3])^T. \quad (4)$$

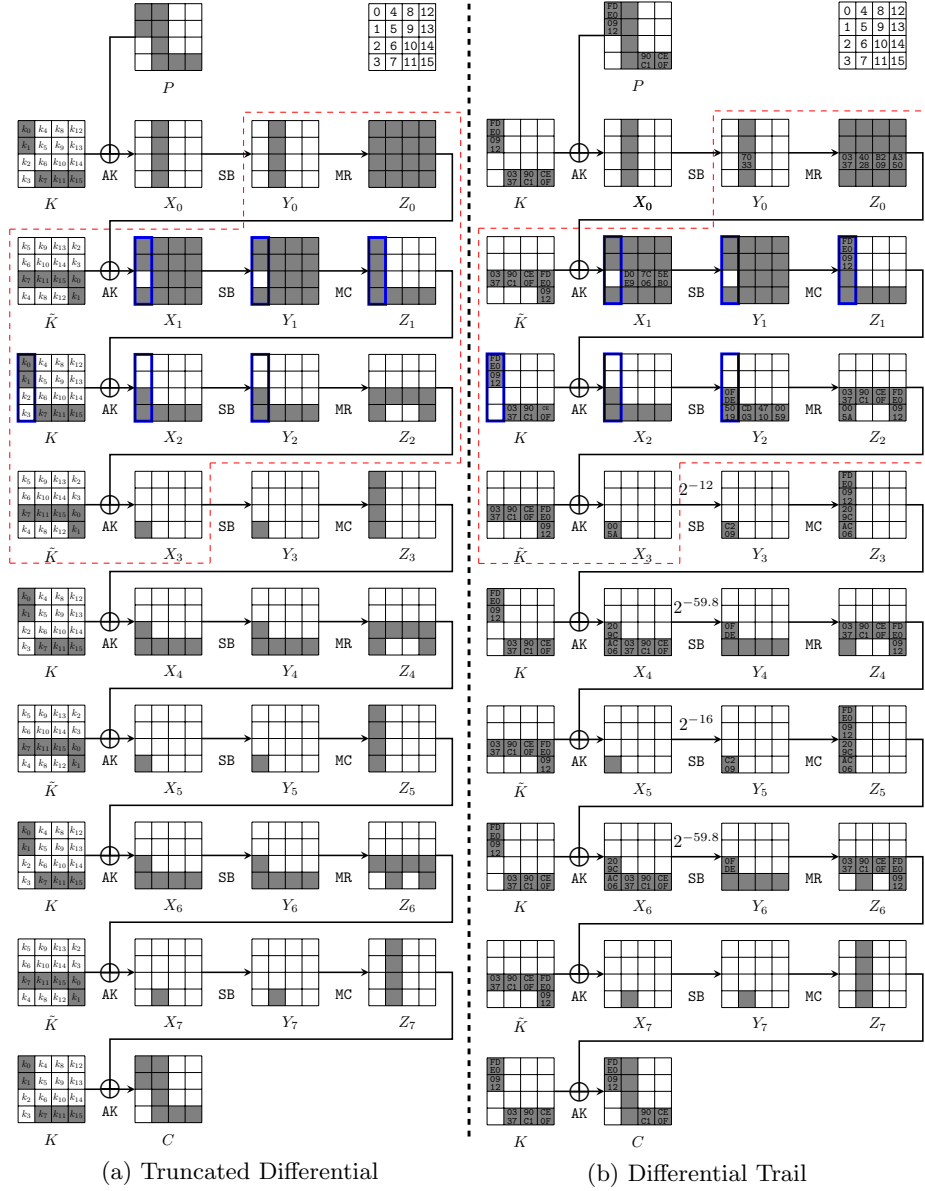


Fig. 10: 8-round Related-key Rebound-attack Trail on Saturnin-hash

The condition of Equation (4) also applies to the computation from ΔY_5 to ΔX_6 . Hence, for Equation (4) and (3), if we fixed Δk_0 , then Δk_7 , Δk_{11} , Δk_{15} , and Δk_1 are determined by Property 1. As shown in Figure 10(a), at Round 0 and 1, $\Delta X_1[2] = \Delta k_7 \oplus \Delta Z_0[2] = 0$, so $\Delta Z_0[2] = \Delta k_7$. From $\Delta Z_0 = \text{MR}(\Delta Y_0)$, for the third row, we have $\Delta Y_0[2, 10, 14] = 0$ and $\Delta Z_0[2] = \Delta k_7$ and Equation (5) is derived. Hence, if Δk_7 is fixed, all other differences in the active cells of ΔY_0

and ΔZ_0 in row 3 are deduce by Property 1.

$$\text{MR}^{-1}(\Delta k_7, \Delta Z_0[6], \Delta Z_0[10], \Delta Z_0[14]) = (0, \Delta Y_0[6], 0, 0). \quad (5)$$

Algorithm 1: Determine the Differences From the Truncated Form

```

1 for  $\Delta k_0 \in \mathbb{F}_2^{16}$  do
2   Deduce  $\Delta k_7, \Delta k_{11}, \Delta k_{15}, \Delta k_1$  by Equation (4) and (3) and Property 1
3   /* All the differences in the key schedule are determined. */
4   Round 2: Deduce  $\Delta Z_2[2, 6, 10, 14], \Delta Y_2[2]$ 
5   Round 3: Deduce  $\Delta Y_3[3]$  by Equation (4) and Property 1. Then
         $Z_3[0, 1, 2, 3]$  and  $X_4[2, 3]$  are fixed.
6   Round 4: Similar to Round 2 to get  $\Delta Z_4[2, 6, 10, 14], \Delta Y_4[2]$ . In addition,
        we have  $\Delta Z_4[15] = \Delta k_1$ 
7   Round 5: Similar to Round 3 to get  $\Delta Y_5[3], Z_5[0, 1, 2, 3]$  and  $X_6[2, 3]$ 
8   Round 6: Similar to Round 2 to get  $\Delta Z_6[2, 6, 10, 14], \Delta Y_6[2]$ . In addition,
        we have  $\Delta Z_6[15] = \Delta k_1$ 
9   Round 0: With Equation (5), we deduce  $\Delta Z_0[6, 10, 14]$  and  $\Delta Y_0[6]$ . Then
         $\Delta X_1[6, 10, 14]$  are determined.
10  Round 1: Since  $\Delta Z_1[0] = \Delta k_0$  and  $\Delta Z_1[1] = \Delta k_1$ ,  $\Delta Z_1[0]$  and  $\Delta Z_1[1]$  is
        fixed.
11  Round 7: In Saturnin-hash (MMO hashing mode), the plaintext is
        XORed into the ciphertext of the internal block cipher to output the
        digest. We have  $T = P \oplus C = X_0 \oplus K \oplus Z_7 \oplus K = X_0 \oplus Z_7$ . Then, if two
        message collide, we have  $\Delta T = 0 = \Delta X_0 \oplus \Delta Z_7$ .
12  As shown in Figure 10(b), from  $\Delta X_4$  to  $\Delta Y_5$ , multiple differential trails
        are taken into account.

```

We derive an 8-round rebound-attack characteristic in Figure 10(b) from the truncated form in Figure 10(a) by Algorithm 1. By traversing $\Delta k_0 \in \mathbb{F}_2^{16}$ in Algorithm 1, we find characteristic with as higher probability as possible. The best trail is given in Figure 10(b), whose total probability of the outbound phase is $2^{-(12+59.8+16+59.8+64)} = 2^{-211.6}$ including the probability of $\Delta X_0 = \Delta Z_7$. In round 4, $2^{-59.8}$ is the total probability of a cluster differential trails from ΔX_4 to ΔZ_4 . The same happens to round 6.

As shown in Figure 10(b), the 2nd, 3rd and 4th super S-boxes are typical non-full-active super S-boxes, where there are only 5 active cells among the 8 input-output cells between MC in round 1 in each super S-box. However, the first super S-box is not a typical one. In fact, between MC in round 1 in the first Super-Sbox, there are one non-active cell and two cells with fixed differences. However, we can regard the two cells with fixed differences as another two “non-active” cells to perform the quantum version of non-full active super S-box technique [18] whose details will be given in Algorithm 2.

For the i th ($i = 0, 1, 2, 3$) non-full-active super S-box, we define $G^{(i)} : \mathbb{F}_2^{16} \times \mathbb{F}_2^3 \mapsto \mathbb{F}_2$ as $G^{(i)}(K, K', \Delta X_1^{(i)}, \Delta Y_2^{(i)}; x, \beta)$, where $x = X_1^{(i)}[0] \in \mathbb{F}_2^{16}$ and $\beta = \beta_0 \parallel \beta_1 \parallel \beta_2 \in \mathbb{F}_2^3$. $G^{(i)}(K, K', \Delta X_1^{(i)}, \Delta Y_2^{(i)}; x, \beta) = 1$ if and only if (x, β) leads to

a valid connection of $(\Delta X_1^{(i)}, \Delta Y_2^{(i)})$ under the key pair (K, K') . The quantum implementation of $\mathcal{U}_{G^{(0)}}$ is given in Algorithm 2.

Complexity of $\mathcal{U}_{G^{(0)}}$ is given in Algorithm 2. The time is bounded by Line 7 to Line 9 of Algorithm 2, which is about (including uncomputing) $3 \times \frac{\pi}{4} \cdot \sqrt{2^{16}} \cdot 2 \cdot 2 = 2^{11.24}$ Sbox evaluations.

Algorithm 2: Implementation of $\mathcal{U}_{G^{(0)}}$ without using qRAMs

Input: $|K, K', \Delta X_1^{(0)}, \Delta Y_2^{(0)}; X_1^{(0)}[0], \beta\rangle |y\rangle$ with $\beta = (\beta_0, \beta_1, \beta_2) \in \mathbb{F}_2^3$
Output: $|K, K', \Delta X_1^{(0)}, \Delta Y_2^{(0)}; X_1^{(0)}[0], \beta\rangle |y \oplus G^{(0)}(K, K', \Delta X_1^{(0)}, \Delta Y_2^{(0)}; X_1^{(0)}[0], \beta)\rangle$

- 1 */* Please focus on the super Sbox marked by blue box in Fig. 10 */*
- 2 $Y_1^{(0)}[0] \leftarrow S(X_1^{(0)}[0])$
- 3 $\Delta Y_1^{(0)}[0] \leftarrow S(X_1^{(0)}[0] \oplus \Delta X_1^{(0)}[0]) \oplus S(X_1^{(0)}[0])$
- 4 Solving the system of equations $\text{MC}(\Delta Y_1^{(0)}) = \Delta Z_1^{(0)}$ with the knowledge of $\Delta Z_1^{(0)}[0] = \text{0xFDE0}$, $\Delta Z_1^{(0)}[1] = \text{0x0912}$ and $\Delta Y_1^{(0)}[2] = 0$
- 5 */* All differences of cells in $\Delta Y_1^{(0)}$, $\Delta Z_1^{(0)}$ are known */*
- 6 Let $g_j : \mathbb{F}_2^{16} \rightarrow \mathbb{F}_2$ be a Boolean function such that $g_j(\delta_{in}, \delta_{out}, \beta_j = 0; x) = 1$ if and only if $S(x) \oplus S(x \oplus \delta_{in}) = \delta_{out}$ and $x \leq x \oplus \delta_{in}$, and $g_j(\delta_{in}, \delta_{out}, \beta_j = 1, x) = 1$ if and only if $S(x) \oplus S(x \oplus \delta_{in}) = \delta_{out}$, and $x > x \oplus \delta_{in}$.
- 7 Run the Grover search on the function $g_0(\Delta X_1^{(0)}[1], \Delta Y_1^{(0)}[1], \beta_0; \cdot) : \mathbb{F}_2^{16} \rightarrow \mathbb{F}_2$.
Let $X_1^{(0)}[1]$ be the output.
- 8 Run the Grover search on the function $g_1(\Delta X_1^{(0)}[3], \Delta Y_1^{(0)}[3], \beta_1; \cdot) : \mathbb{F}_2^{16} \rightarrow \mathbb{F}_2$.
Let $X_1^{(0)}[3]$ be the output.
- 9 Run the Grover search on the function $g_2(\Delta X_2^{(0)}[3], \Delta Y_2^{(0)}[3], \beta_2; \cdot) : \mathbb{F}_2^{16} \rightarrow \mathbb{F}_2$.
Let $X_2^{(0)}[3]$ be the output.
- 10 Compute $Y_1^{(0)}[1]$, $Y_1^{(0)}[3]$ and $Z_1^{(0)}[3]$; */* $Y_1^{(0)}[0]$ is known */*
- 11 Solve the equation $\text{MC}(Y_1^{(0)}) = Z_1^{(0)}$ for other unknown cells, i.e., $Y_1^{(0)}[2]$, $Z_1^{(0)}[0, 1, 2]$, and $X_1^{(0)}$
- 12 */* the value $Y_1^{(0)}$ is known */*
- 13 **if** $S(Z_1^{(0)}[2] \oplus \Delta Z_1^{(0)}[2] \oplus K'[2]) \oplus S(Z_1^{(0)}[2] \oplus K[2]) = \Delta Y_2^{(0)}[2]$ **then**
- 14 **return** $|K, K', \Delta X_1^{(0)}, \Delta Y_2^{(0)}; X_1^{(0)}[0], \beta\rangle |y \oplus 1\rangle$
- 15 **else**
- 16 **return** $|K, K', \Delta X_1^{(0)}, \Delta Y_2^{(0)}; X_1^{(0)}[0], \beta\rangle |y\rangle$

Since the probability of the outbound phase is $2^{-211.6}$, after traversing $2^{211.6}$ starting points computed by the inbound phase, it is expected to find one collision. Given the key difference $\Delta K = K \oplus K'$, there are 2^{256} valid key pairs (K, K') . Hence, we have enough degrees of freedom to find the collision. For

simplicity, we just fix the input difference ΔX_1 of the inbound phase and compute the starting points by traversing a 212-bit K to find the collision. Define $F : \mathbb{F}_2^{212} \times \mathbb{F}_2^3 \mapsto \mathbb{F}_2$ as $F(\Delta K, \Delta X_1, \Delta Y_2; x, \alpha)$, where $x = K \in \mathbb{F}_2^{212}$ and $\alpha = \alpha_0 \parallel \alpha_1 \parallel \alpha_2 \in \mathbb{F}_2^3$. $F(\Delta K, \Delta X_1, \Delta Y_2; x, \alpha) = 1$ if and only if $(\Delta K, \Delta X_1, \Delta Y_2; x, \alpha)$ leads a collision. The implementation of \mathcal{U}_F is given in Algorithm 3.

Algorithm 3: Implementation of \mathcal{U}_F without using qRAMs

Input: $|\Delta K, \Delta X_1, \Delta Y_2; K, \alpha\rangle |y\rangle$ with $\alpha = (\alpha_0, \alpha_1, \alpha_2) \in \mathbb{F}_2^3$
Output: $|\Delta K, \Delta X_1, \Delta Y_2; K, \alpha\rangle |y \oplus F(\Delta K, \Delta X_1, \Delta Y_2; K, \alpha)\rangle$

- 1 Compute $K' = K \oplus \Delta K$
- 2 **for** $i \in \{0, 1, 2\}$ **do**
- 3 Derive the $\Delta X_1^{(i)}$ and $\Delta Y_2^{(i)}$ for $\text{SSB}^{(i)}$ from the ΔX_1 and ΔY_2
- 4 Run Grover search on the function $G^{(i)}(K, K', \Delta X_1^{(i)}, \Delta Y_2^{(i)}; \cdot) : \mathbb{F}_2^{19} \mapsto \mathbb{F}_2$.
 Let $X_1^{(i)}[0] \in \mathbb{F}_2^{16}$, $\beta^{(i)} \in \mathbb{F}_2^3$ be the output.
- 5 Run Line 2 to Line 11 of Algorithm 2 with $X_1^{(i)}[0] \in \mathbb{F}_2^{16}$, $\beta^{(i)} \in \mathbb{F}_2^3$ as
 input. Let $X_1^{(i)}$ as output.
- 6 Let $\tilde{X}_1^{(i)} = \max\{X_1^{(i)}, X_1^{(i)} \oplus \Delta X_1^{(i)}\}$ if $\alpha_i = 0$, else
 $\tilde{X}_1^{(i)} = \min\{X_1^{(i)}, X_1^{(i)} \oplus \Delta X_1^{(i)}\}$
- 7 Derive the $\Delta X_1^{(3)}$ and $\Delta Y_2^{(3)}$ for $\text{SSB}^{(3)}$ from the ΔX_1 and ΔY_2
- 8 Run Grover search on the function $G^{(3)}(K, K', \Delta X_1^{(3)}, \Delta Y_2^{(3)}; \cdot) : \mathbb{F}_2^{19} \mapsto \mathbb{F}_2$.
 Let $X_1^{(3)}[0] \in \mathbb{F}_2^{16}$, $\beta^{(3)} \in \mathbb{F}_2^3$ be the output.
- 9 Run Line 2 to Line 11 of Algorithm 2 with $X_1^{(3)}[0] \in \mathbb{F}_2^{16}$, $\beta^{(3)} \in \mathbb{F}_2^3$ as input.
 Let $X_1^{(3)}$ as output.
- 10 Let $\tilde{X}_1^{(3)} = \max\{X_1^{(i)}, X_1^{(i)} \oplus \Delta X_1^{(i)}\}$
- 11 /* Create the starting point (K, X_1) with $(\Delta K, \Delta X_1, \Delta Y_2)$ */
- 12 $X_1 \leftarrow (\tilde{X}_1^{(0)}, \tilde{X}_1^{(1)}, \tilde{X}_1^{(2)}, \tilde{X}_1^{(3)})$
- 13 $X_1' \leftarrow X_1 \oplus \Delta X_1$
- 14 Compute forward and backward to the beginning and ending of the 8-round
 trail from (X_1, X_1') with (K, K')
- 15 **if** (X_1, X_1') and (K, K') lead to a collision **then**
- 16 | return $|\Delta K, \Delta X_1, \Delta Y_2; K, \alpha\rangle |y \oplus 1\rangle$
- 17 **else**
- 18 | return $|\Delta K, \Delta X_1, \Delta Y_2; K, \alpha\rangle |y\rangle$

Complexity of \mathcal{U}_F in Algorithm 3. There are four Grover searches on $G^{(i)}$ in Line 4 and 8. There are four calls of Algorithm 2 in Line 5 and Line 9. Those procedures bound the time complexity of \mathcal{U}_F as $4 \cdot \frac{\pi}{4} \cdot \sqrt{2^{19}} \cdot 2^{11.24} + 4 \cdot 2^{11.24} = 2^{22.39}$ S-box evaluations.

To find the collision on 8-round **Saturnin-hash**, we apply Grover search on $F(\Delta K, \Delta X_1, \Delta Y_2; \cdot) : \mathbb{F}_2^{212+3} \mapsto \mathbb{F}_2$ with \mathcal{U}_F in Algorithm 3, which costs

$$\frac{\pi}{4} \cdot \sqrt{2^{212+3}} \cdot 2^{22.39} = 2^{129.54} \quad \text{S-box evaluations.}$$

Since there are $16 \times 8 = 128$ Sbox applications, the time complexity to find the collision is about $2^{129.54}/128 = 2^{122.54}$ 8-round **Saturnin-hash**.

In our full version paper, we also present a 7-round quantum collision attack, a 5-round classical collision attack and a 6-round classical free-start collision attack, and a 7-round quantum semi-free-start collision on **Saturnin-hash**.

5 Free-Start Collision on reduced SKINNY- $n-3n$ -MMO/MP

SKINNY is a family of lightweight block ciphers designed by Beierle et al. [3]. In this section, we apply our method to SKINNY- $n-3n$. Please find the structure of SKINNY- $n-3n$ in [3] or our full version paper. The MC operation is non-MDS:

$$\text{MC} \begin{pmatrix} a \\ b \\ c \\ d \end{pmatrix} = \begin{pmatrix} a \oplus c \oplus d \\ a \\ b \oplus c \\ a \oplus c \end{pmatrix} \quad \text{and} \quad \text{MC}^{-1} \begin{pmatrix} \alpha \\ \beta \\ \gamma \\ \delta \end{pmatrix} = \begin{pmatrix} \beta \\ \beta \oplus \gamma \oplus \delta \\ \beta \oplus \delta \\ \alpha \oplus \delta \end{pmatrix}. \quad (6)$$

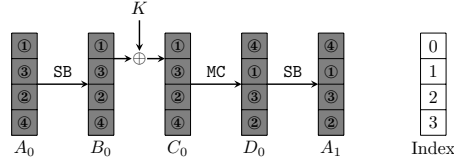


Fig. 11: Super S-box with SKINNY's non-MDS matrix

Since SKINNY applies non-MDS matrix in MC, we will adapt the method of super S-box technique for SKINNY. Different from the super S-box technique with MDS matrix [21,38], we do not need to an exponential memory to store the differential distribution of the super S-box, which is friendly to quantum attacks.

5.1 Super S-box with Non-MDS Matrix

As shown in Figure 11 (SR is omitted), the circled numbers indicate the computation sequence. When computing the super S-box, the key pair is fixed, i.e., K and K' are known.

1. In step ①, we have $D_0[1] = C_0[0]$ due to Equation (6), then we have

$$\begin{aligned} \Delta A_1[1] &= \mathbf{S}(D_0[1]) \oplus \mathbf{S}(D'_0[1]) \\ &= \mathbf{S}(C_0[0]) \oplus \mathbf{S}(C'_0[0]) = \mathbf{S}(\mathbf{S}(A_0[0]) \oplus K[0]) \oplus \mathbf{S}(\mathbf{S}(A'_0[6]) \oplus K'[0]) \\ &= \mathbf{S}(\mathbf{S}(A_0[0]) \oplus K[0]) \oplus \mathbf{S}(\mathbf{S}(A_0[0]) \oplus \Delta A_0[0]) \oplus K'[0]. \end{aligned} \quad (7)$$

Hence, given input-output differences $(\Delta A_0[0], \Delta A_1[1])$, we compute one conforming value of $A_0[0]$ that satisfy Equation (7) by traversing a space of 2^c for $A_0[0]$. After that, all cells marked by “①” are determined.

2. In step ②, we have $D_0[3] = C_0[0] \oplus C_0[2]$ due to Equation (6), then we have

$$\begin{aligned} \Delta A_1[3] &= \mathbf{s}(D_0[3]) \oplus \mathbf{s}(D'_0[3]) = \mathbf{s}(C_0[0] \oplus C_0[2]) \oplus \mathbf{s}(C'_0[0] \oplus C'_0[2]) \\ &= \mathbf{s}(\mathbf{s}(A_0[0]) \oplus K[0] \oplus \mathbf{s}(A_0[2])) \oplus \mathbf{s}(\mathbf{s}(A'_0[0]) \oplus K'[0] \oplus \mathbf{s}(A'_0[2])) \\ &= \mathbf{s}(\mathbf{s}(A_0[0]) \oplus K[0] \oplus \mathbf{s}(A_0[2])) \oplus \mathbf{s}(\mathbf{s}(A_0[0] \oplus \Delta A_0[0]) \oplus K'[0] \oplus \mathbf{s}(A_0[2] \oplus \Delta A_0[2])). \end{aligned} \quad (8)$$

Since all the input-output differences of the super S-box and the pair of K are fixed, and $A_0[0]$ is determined by in step ①, only $A_0[2]$ is unfixed. We search $A_0[2]$ in a space of 2^8 to find the right one that make Equation (8) holds. All cells marked by “②” are fixed.

3. In step ③, we have $D_0[2] = C_0[1] \oplus C_0[2]$ due to Equation (6), then we have

$$\begin{aligned} \Delta A_1[2] &= \mathbf{s}(D_0[2]) \oplus \mathbf{s}(D'_0[2]) \\ &= \mathbf{s}(C_0[1] \oplus C_0[2]) \oplus \mathbf{s}(C'_0[1] \oplus C'_0[2]) \\ &= \mathbf{s}(\mathbf{s}(A_0[1]) \oplus K[1] \oplus \mathbf{s}(A_0[2])) \oplus \mathbf{s}(\mathbf{s}(A'_0[1]) \oplus K'[1] \oplus \mathbf{s}(A'_0[2])) \\ &= \mathbf{s}(\mathbf{s}(A_0[1]) \oplus K[1] \oplus \mathbf{s}(A_0[2])) \oplus \mathbf{s}(\mathbf{s}(A_0[1] \oplus \Delta A_0[1]) \oplus K'[1] \oplus \mathbf{s}(A_0[2] \oplus \Delta A_0[2])). \end{aligned} \quad (9)$$

Since all the input-output differences of the super S-box and the pair of K are fixed, and $A_0[2]$ is determined by in step ②, only $A_0[1]$ is unfixed. We search $A_0[1]$ in a space of 2^8 to find the right one that make Equation (9) holds. All cells marked by “③” are fixed.

4. In step ④, we have $D_0[0] = C_0[0] \oplus C_0[2] \oplus C_0[3]$ due to Equation (6), then we have

$$\begin{aligned} \Delta A_1[0] &= \mathbf{s}(D_0[0]) \oplus \mathbf{s}(D'_0[0]) \\ &= \mathbf{s}(C_0[0] \oplus C_0[2] \oplus C_0[3]) \oplus \mathbf{s}(C'_0[0] \oplus C'_0[2] \oplus C'_0[3]) \\ &= \mathbf{s}(\mathbf{s}(A_0[0]) \oplus K[0] \oplus \mathbf{s}(A_0[2]) \oplus \mathbf{s}(A_0[3])) \oplus \mathbf{s}(\mathbf{s}(A'_0[0]) \oplus K'[0] \oplus \mathbf{s}(A'_0[2]) \oplus \mathbf{s}(A'_0[3])) \\ &= \mathbf{s}(\mathbf{s}(A_0[0]) \oplus K[0] \oplus \mathbf{s}(A_0[2]) \oplus \mathbf{s}(A_0[3])) \oplus \\ &\quad \mathbf{s}(\mathbf{s}(A_0[0] \oplus \Delta A_0[0]) \oplus K'[0] \oplus \mathbf{s}(A_0[2] \oplus \Delta A_0[2]) \oplus \mathbf{s}(A_0[3] \oplus \Delta A_0[3])). \end{aligned}$$

Since all the input-output differences of the super S-box and the pair of K are fixed, and $A_0[0]$ and $A_0[2]$ are already determined by in step ② and ③, only $A_0[3]$ is unfixed. We search $A_0[3]$ in a space of 2^8 to find the right one that make Equation (9) holds. All cells marked by “④” are fixed.

Following the above computing order, given an input-output difference $(\Delta A_0, \Delta A_1)$ with fixed key pair, we find the conforming pair for the full active super S-box in time complexity of about 2^8 two-round computations without any memory. Note that if the MC operation adopts MDS matrix, without memory, we need 2^{32} classical time to find a conforming pair for full active super S-box.

5.2 Collision on Hashing Modes with Reduced SKINNY-128-384

By applying the model given in Section 3, we find 16-round rebound trail for SKINNY-128-384 (see Figure 19 in our full version paper). The inbound phase covers round 11 and round 12. The probability of the outbound phase is 2^{-112} . We apply similar technique of super S-box with non-MDS matrix to the inbound phase of the 16-round rebound trail, whose quantum time complexity is about

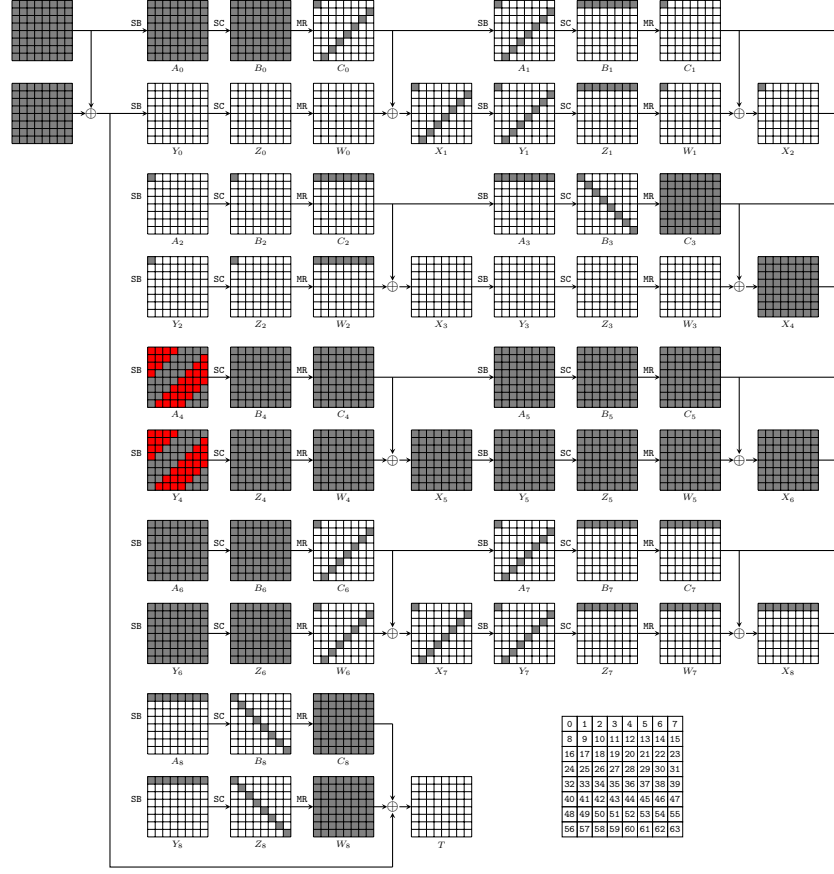


Fig. 12: Free-start collision attack on 9-round Whirlpool

$2^{8.65}$ S-box evaluations. To be more clear, we list the details for solving the inbound phase in Section D in our full version paper.

Define $F : \mathbb{F}_2^{112} \times \mathbb{F}_2^3 \mapsto \mathbb{F}_2$ as $F(\Delta K, \Delta X_{11}, \Delta Y_{12}; x, \alpha)$, where $x = K \in \mathbb{F}_2^{112}$ and $\alpha = \alpha_0 \parallel \alpha_1 \parallel \alpha_2 \in \mathbb{F}_2^3$. $F(\Delta K, \Delta X_{11}, \Delta Y_{12}; x, \alpha) = 1$ if and only if $(\Delta K, \Delta X_{11}, \Delta Y_{12}; x, \alpha)$ leads a collision. The overall time complexity is

$$\frac{\pi}{4} \cdot \sqrt{2^{112+3}} \cdot 4 \cdot 2^{8.65} = 2^{67.8} \quad \text{S-box evaluations,}$$

which is about $2^{67.8}/256 = 2^{59.8}$ 16-round SKINNY-128-384, since there are 256 S-boxes in the 16-round SKINNY-128-384.

6 Free-Start Collision Attack on 9-Round Whirlpool

Different from Saturnin and SKINNY, the key schedule of Whirlpool is nonlinear. Hence, we have to tweak the automatic tool in Section 3 which targets on linear

key schedule ciphers. For `Whirlpool`, we place the rebound attacks in both the encryption data path and the key schedule path just like Sasaki et al.’s work [49]. For the inbound part of the key schedule path, we only have input and output differences Δ_{in}^K and Δ_{out}^K that act as the degrees of freedom to preform the rebound attack in the key. We expect to get $|\Delta_{in}^K| \cdot |\Delta_{out}^K|$ key pairs conforming to the inbound part of key schedule path. For each key pair, we will get $|\Delta_{in}^E| \cdot |\Delta_{out}^E|$ pairs conforming to the inbound part of the encryption data path. Suppose the total probability of outbound paths in the key and encryption path is p , then the condition $|\Delta_{in}^K| \cdot |\Delta_{out}^K| \cdot |\Delta_{in}^E| \cdot |\Delta_{out}^E| \geq 1/p$ should be satisfied to finally find a key pair and data pair fulfilling the whole trails in the key schedule and the encryption data path. We embed the 2-round full/non-full active super S-box technique [21,48] or 3-round-inbound technique [30] in the inbound part. The inbound phase in related-key setting is quite similar to the single-key setting. A slight different point is to deal with the operation of XOR the key difference into the internal state, where the constraint [42] for truncated differential in XOR operation is applied. The outbound phase is also similar to single-key setting, where only propagations of truncated differential are constrained with MILP.

At ASIACRYPT 2012, Sasaki et al. [49] introduced a free-start collision attack on 8-round `Whirlpool`. In this section, we find a new 9-round rebound characteristic in Figure 12, and based on it, we give the quantum free-start collision on 9-round `Whirlpool`.

6.1 Comparison between Sasaki et al’s Trail and Ours

The number of active S-boxes in Sasaki et al’s 8-round trail is shown below:

$$\begin{cases} Key : 64 \xrightarrow{1^{st}R} 8 \xrightarrow{2^{nd}R} 1 \xrightarrow{3^{rd}R} 8 \xrightarrow{4^{th}R} 64 \xrightarrow{5^{th}R} 8 \xrightarrow{6^{th}R} 1 \xrightarrow{7^{th}R} 8 \xrightarrow{8^{th}R} 64, \\ Data : 0 \xrightarrow{1^{st}R} 8 \xrightarrow{2^{nd}R} 1 \xrightarrow{3^{rd}R} 8 \xrightarrow{4^{th}R} 0 \xrightarrow{5^{th}R} 8 \xrightarrow{6^{th}R} 1 \xrightarrow{7^{th}R} 8 \xrightarrow{8^{th}R} 64. \end{cases}$$

The number of active S-boxes in our 9-round trail is shown below:

$$\begin{cases} Key : 64 \xrightarrow{1^{st}R} 8 \xrightarrow{2^{nd}R} 1 \xrightarrow{3^{rd}R} 8 \xrightarrow{4^{th}R} 64 \xrightarrow{5^{th}R} 64 \xrightarrow{6^{th}R} 64 \xrightarrow{7^{th}R} 8 \xrightarrow{8^{th}R} 8 \xrightarrow{9^{th}R} 64, \\ Data : 0 \xrightarrow{1^{st}R} 8 \xrightarrow{2^{nd}R} 1 \xrightarrow{3^{rd}R} 0 \xrightarrow{4^{th}R} 64 \xrightarrow{5^{th}R} 64 \xrightarrow{6^{th}R} 64 \xrightarrow{7^{th}R} 8 \xrightarrow{8^{th}R} 8 \xrightarrow{9^{th}R} 64. \end{cases}$$

In the key schedule, Sasaki et al’s inbound phase “ $8 \xrightarrow{4^{th}R} 64 \xrightarrow{5^{th}R} 8$ ” is replaced by a longer inbound phase “ $8 \xrightarrow{4^{th}R} 64 \xrightarrow{5^{th}R} 64 \xrightarrow{6^{th}R} 64 \xrightarrow{7^{th}R} 8$ ” in our trail, namely we gain a 2-round extension in the inbound phase. In the meantime, Sasaki et al.’s outbound part “ $8 \xrightarrow{6^{th}R} 1 \xrightarrow{7^{th}R} 8 \xrightarrow{8^{th}R} 64$ ” is shortened to “ $8 \xrightarrow{8^{th}R} 8 \xrightarrow{9^{th}R} 64$ ” to gain enough degrees of freedom. In Sasaki et al.’s 8-round trail, the full active state to match in the inbound phase only happens to the key schedule data path. In the inbound part of the encryption data path, many cells are inactive, so that one can assign arbitrary values. Hence, we do not worry about the degree of freedom for Sasaki et al.’s trail. However, in our 9-round trail, both the key and data path adopt full state active inbound part, so that the internal states are fully determined by a match-in-the-middle approach and the degree of freedoms

only comes from the possible input and output differences of the inbound part. Hence, the outbound phase is different to gain enough degrees of freedom for the collision attack.

In the key schedule path, the inbound part covers from ΔB_3 to ΔC_6 that includes 3 SB layers. We apply Jean et al.'s [30] 3-round-inbound technique and their quantum version by Hosoyamada and Sasaki [26] to perform the attack. We first define G in Algorithm 4 which marks the compatible \blacksquare cells in Figure 4 for (X_1, X'_1) for a given input difference ΔX_1 and output difference ΔY_3 .

Complexity of \mathcal{U}_G in Algorithm 4. Taken uncomputing into account, there are $32 \times 2 \times 2 \times 2 = 128$ S-boxes operations in Line 3. In Line 5 to Line 8, we need $8 \cdot \frac{\pi}{4} \cdot \sqrt{2^{64}} \cdot 16 \times 2 = 2^{39.65}$ S-boxes operations.

In Line 10 of Algorithm 4, only the \blacksquare cells are needed to compute backward to X_1 , hence, $32 \times 2 \times 2 \times 2 = 128$ S-boxes operations are needed. Totally, we need about $2^{39.65}$ S-boxes operations to implement \mathcal{U}_G .

Given $(\Delta X_1, \Delta Y_3)$, run Grover's algorithm on \mathcal{U}_G to find the correct \blacksquare cells for (X_1, X'_1) in Figure 4. \mathcal{U}_G outputs 1 with probability of 2^{-256} . Hence, the time complexity to find the correct value with Grover's algorithm is

$$\frac{\pi}{4} \cdot \sqrt{2^{256}} \cdot 2^{39.65} = 2^{167.3} \text{ S-boxes operations.} \quad (10)$$

6.2 Free-Start Collision on 9-round Whirlpool

Classical Analysis on the 9-round Rebound Trail. As shown in Figure 12, in the key schedule part, given an input-output difference ΔB_3 and ΔC_6 of the inbound part, we have one conforming pair on average. In the outbound phase of the key schedule, the probability that the truncated differential ΔC_2 propagates to ΔB_2 is 2^{-56} . Hence, there will be $2^{64 \times 2 - 56} = 2^{72}$ valid key pairs that meet the truncated differential in the key schedule path. For each valid key pair, we look at the encryption data path. ΔX_4 is fixed by ΔC_3 , and there are 2^{64} possible differences in ΔW_6 . There is also a 3-round inbound phase in the encryption data path with input difference ΔX_4 and output difference ΔW_6 . With a given $(\Delta X_4, \Delta W_6)$, it is expected to find one data pair (X_4, X'_4) . Together with the key pair, we compute backward with the data pair (X_4, X'_4) . Since $\Delta W_2 = \Delta C_2$ and $\Delta B_2 = \text{MR}^{-1}(\Delta C_2)$ whose row 0 is of $(*, 0, 0, 0, 0, 0, 0, 0)$, ΔZ_2 is also of the truncated form $(*, 0, 0, 0, 0, 0, 0, 0)$ with probability 1. At round 0, $\Delta W_0 = \Delta C_0 \oplus \Delta X_1 = 0$ holds with probability of 2^{-64} . At the last round, $\Delta B_8 = \Delta Z_8$ holds with probability 2^{-64} , which finally leads to a collision. The total degrees of freedom are derived from ΔB_3 , ΔC_6 and ΔW_6 , which consists of 2^{192} possible differences (24-byte). The probability to generate a collision is $2^{-56-128} = 2^{-184}$. The classical time complexity to solve the 3-round inbound phase is about 2^{320} . Obviously, the classical complexity will be much larger than a generic birthday attack, which only needs 2^{256} time to find the 512-bit collision.

Quantum Free-Start Collision Attack on 9-round Whirlpool. In the key schedule path, for given $C_6[\mathbb{U}]$ with $\mathbb{U} = \{0, 15, 22, 29, 36, 43, 50, 57\}$ positions of

Algorithm 4: Implementation of \mathcal{U}_G without using qRAMs

Input: $|\Delta X_1, \Delta Y_3; X_1[\blacksquare]\rangle |y\rangle$
Output: $|\Delta X_1, \Delta Y_3; X_1[\blacksquare]\rangle |y \oplus G(\Delta X_1, \Delta Y_3; X_1[\blacksquare])\rangle$

- 1 /* $X_1[\blacksquare]$ means the value of 32 \blacksquare cells in state X_1 shown in Figure 4, and $X'_1[\blacksquare]$ is for state X'_1 */
- 2 Compute $X'_1[\blacksquare] = \Delta X_1 \oplus X_1[\blacksquare]$
- 3 Compute $Z_2[\blacksquare]$ and $Z'_2[\blacksquare]$ by $X_1[\blacksquare]$ and $X'_1[\blacksquare]$, respectively
- 4 Define $g_j : \mathbb{F}_2^{8 \times 8} \mapsto \mathbb{F}_2$ for row $j = 0, 1, 2, \dots, 7$ of Z_2 . E.g., for row 0, define $g_0(Z_2[\blacksquare], Z'_2[\blacksquare]; x)$, where x is the \blacksquare cells of Z_2 and Z'_2 in row 0, i.e., $x = Z_2[1, 2, 3, 4] \| Z'_2[1, 2, 3, 4] \in \mathbb{F}_2^{8 \times 8}$. $g_0(Z_2[\blacksquare], Z'_2[\blacksquare]; x) = 1$ if and only if $\text{SB}(\text{MR}(Z_2[0, 1, \dots, 7])) \oplus \text{SB}(\text{MR}(Z'_2[0, 1, \dots, 7])) = \Delta Y_3[0, 1, \dots, 7]$. Similar property holds for other g_j
- 5 Run the Grover search on $g_0(Z_2[\blacksquare], Z'_2[\blacksquare]; \cdot) : \mathbb{F}_2^{8 \times 8} \mapsto \mathbb{F}_2$. Let $Z_2[1, 2, 3, 4] \| Z'_2[1, 2, 3, 4]$ be the output.
- 6 Run the Grover search on $g_1(Z_2[\blacksquare], Z'_2[\blacksquare]; \cdot) : \mathbb{F}_2^{8 \times 8} \mapsto \mathbb{F}_2$. Let $Z_2[10, 11, 12, 13] \| Z'_2[10, 11, 12, 13]$ be the output.
- 7 \vdots
- 8 Run the Grover search on $g_7(Z_2[\blacksquare], Z'_2[\blacksquare]; \cdot) : \mathbb{F}_2^{8 \times 8} \mapsto \mathbb{F}_2$. Let $Z_2[56, 57, 58, 59] \| Z'_2[56, 57, 58, 59]$ be the output.
- 9 /* Now the whole states Z_2 and Z'_2 are fixed. */
- 10 Compute backward from Z_2 and Z'_2 to X_1 and X'_1
- 11 **if** $X_1[\blacksquare] \oplus X'_1[\blacksquare] = \Delta X_1[\blacksquare]$ **then**
- 12 | return $|\Delta X_1, \Delta Y_3; X_1[\blacksquare]\rangle |y \oplus 1\rangle$
- 13 **else**
- 14 | return $|\Delta X_1, \Delta Y_3; X_1[\blacksquare]\rangle |y\rangle$

active cells in C_6 , we define $f : \mathbb{F}_2^{8 \times 8} \mapsto \mathbb{F}_2$ as $f(\Delta C_6[\mathbb{U}]; x)$, where $x = \Delta B_3[\mathbb{V}] \in \mathbb{F}_2^{8 \times 8}$ with $\mathbb{V} = \{0, 9, 18, 27, 36, 45, 54, 63\}$. $f(\Delta C_6[\mathbb{U}]; x) = 1$ if and only if the key pair derived by solving the 3-round inbound satisfies the truncated differential from ΔC_2 to ΔB_2 . The implementation of \mathcal{U}_f is given in Algorithm 5.

Complexity of \mathcal{U}_f . The time is bounded by Line 2 of Algorithm 5, which is about $2^{167.3}$ S-boxes operations according to Equation (10).

Run Grover's algorithm on $f(\Delta C_6[\mathbb{U}]; \cdot)$, we will find a key pair (K, K') that conforms to the truncated differential in Figure 12. In encryption data path, for the computed key pair (K, K') , we define $\tilde{f} : \mathbb{F}_2^{8 \times 8} \mapsto \mathbb{F}_2$ as $\tilde{f}(K, K'; x)$, where $x = \Delta W_6[\mathbb{U}] \in \mathbb{F}_2^{8 \times 8}$. $\tilde{f}(K, K'; x) = 1$ if and only if a collision occurs in the digest that happens with probability of 2^{-128} . The implementation of $\mathcal{U}_{\tilde{f}}$ is given in Algorithm 6.

Complexity of $\mathcal{U}_{\tilde{f}}$. The time complexity is bounded by Line 3 of Algorithm 6, which is also $2^{167.3}$ S-boxes operations according to Equation (10).

We define $F : \mathbb{F}_2^{8 \times 8} \mapsto \mathbb{F}_2$ as $F(x)$, where $x = \Delta C_6[\mathbb{U}] \in \mathbb{F}_2^{8 \times 8}$ with $\mathbb{U} = \{0, 15, 22, 29, 36, 43, 50, 57\}$. $F(x) = 1$ if and only if the digests of two messages collide. The implementation of \mathcal{U}_F is given in Algorithm 7.

Algorithm 5: \mathcal{U}_f of the quantum attack on 9-round Whirlpool

Input: $|\Delta C_6[\mathbb{U}]; \Delta B_3[\mathbb{V}]\rangle |y\rangle$
Output: $|\Delta C_6[\mathbb{U}]; \Delta B_3[\mathbb{V}]\rangle |y \oplus f(\Delta C_6[\mathbb{U}]; \Delta B_3[\mathbb{V}])\rangle$

- 1 Compute ΔC_3 and ΔA_6 from $\Delta B_3[\mathbb{V}]$ and $\Delta C_6[\mathbb{U}]$
- 2 Run Grover's algorithm on $G(\Delta C_3, \Delta A_6; \cdot)$ with \mathcal{U}_G implemented in Algorithm 4. Let $A_4[\blacksquare]$ be the output
- 3 /* $A_4[\blacksquare]$ are the \blacksquare cells in A_4 in Figure 12 */
- 4 Run Line 2 to Line 10 of Algorithm 4 with input $(\Delta C_3, \Delta A_6; A_4[\blacksquare])$. Let (C_3, C'_3) be the output
- 5 Compute backward from (C_3, C'_3) to (B_2, B'_2)
- 6 if row 0 of ΔB is of the truncated form $(*, 0, 0, 0, 0, 0, 0)$ then
 - 7 | return $|\Delta C_6[\mathbb{U}]; \Delta B_3[\mathbb{V}]\rangle |y \oplus 1\rangle$
- 8 else
 - 9 | return $|\Delta C_6[\mathbb{U}]; \Delta B_3[\mathbb{V}]\rangle |y\rangle$

Algorithm 6: $\mathcal{U}_{\tilde{f}}$ of the quantum attack on 9-round Whirlpool

Input: $|K, K'; \Delta W_6[\mathbb{U}]\rangle |y\rangle$
Output: $|K, K'; \Delta W_6[\mathbb{U}]\rangle |y \oplus \tilde{f}(K, K'; \Delta W_6[\mathbb{U}])\rangle$

- 1 Compute ΔX_4 from (K, K')
- 2 Compute ΔY_6 from $\Delta W_6[\mathbb{U}]$
- 3 Run Grover's algorithm on $G(\Delta X_4, \Delta Y_6; \cdot)$ with \mathcal{U}_G implemented in Algorithm 4. Let $Y_4[\blacksquare]$ be the output
- 4 /* $Y_4[\blacksquare]$ are the \blacksquare cells in Y_4 in Figure 12 */
- 5 Run Line 2 to Line 10 of Algorithm 4 with input $(\Delta X_4, \Delta Y_6, Y_4[\blacksquare])$. Let (X_4, X'_4) be output
- 6 Together with (K, K') , compute backward from (X_4, X'_4) to (X_1, X'_1) and forward to (W_8, W'_8)
- 7 Compute (C_0, C'_0) and (C_8, C'_8) by (K, K')
- 8 if $\Delta X_1 = \Delta C_0$ and $\Delta W_8 = \Delta C_8$ then
 - 9 | return $|K, K'; \Delta W_6[\mathbb{U}]\rangle |y \oplus 1\rangle$
- 10 else
 - 11 | return $|K, K'; \Delta W_6[\mathbb{U}]\rangle |y\rangle$

Complexity of \mathcal{U}_F . The time complexity of the implementation of \mathcal{U}_F in Algorithm 7 is bounded by Line 1 and Line 4, which is $\frac{\pi}{4} \cdot \sqrt{2^{64-8}} \cdot 2^{167.3} + \frac{\pi}{4} \cdot \sqrt{2^{64}} \cdot 2^{167.3} = 2^{199.04}$ S-boxes operations.

\mathcal{U}_F returns $|\Delta C_6[\mathbb{U}]\rangle |y \oplus 1\rangle$ with probability of $2^{64-128} = 2^{-64}$. Hence, applying Grover's algorithm on $F(x)$ will finally find the collision. Since only the correct state $\Delta C_6[\mathbb{U}]$ is output, we have to re-run Line 1 to Line 6 of Algorithm 7 to finally find the collision. The total time complexity is bounded by the step of applying Grover's algorithm on $F(x)$, which is

$$\frac{\pi}{4} \cdot \sqrt{2^{64}} \cdot 2^{199.04} = 2^{230.7} \text{ S-boxes operations.}$$

Since there are $128 \times 9 = 1152$ S-boxes operations in the 9-round Whirlpool, the total time complexity of the attack is $2^{230.7}/1152 = 2^{220.5}$ 9-round Whirlpool.

Algorithm 7: \mathcal{U}_F of the quantum attack on 9-round Whirlpool

Input: $|\Delta C_6[\mathbb{U}]\rangle |y\rangle$
Output: $|\Delta C_6[\mathbb{U}]\rangle |y \oplus F(\Delta C_6[\mathbb{U}])\rangle$

- 1 Run Grover's algorithm on $f(\Delta C_6[\mathbb{U}]; \cdot)$ with implementation of \mathcal{U}_f in Algorithm 5. Let $\Delta B_3[\mathbb{V}]$ as output
- 2 /* Note that the truncated differential ΔC_2 to ΔB_2 holds with probability of 2^{-56} , hence, about $\frac{\pi}{4}\sqrt{2^{56}}$ Grover iterations on $f(\Delta C_6[\mathbb{U}]; \cdot)$ are needed to find a good one. */
- 3 Run Line 1 to Line 5 of Algorithm 5 to get (C_3, C'_3) , then compute the key pair (K, K')
- 4 Run Grover's algorithm on $\tilde{f}(K, K'; \cdot)$ with implementation of $\mathcal{U}_{\tilde{f}}$ in Algorithm 6. Let $\Delta W_6[\mathbb{U}]$ as output
- 5 /* Note that since $\mathcal{U}_{\tilde{f}}$ returns 1 with probability of 2^{-128} , however, the size of its domain is 2^{64} . Then after 2^{32} Grover iterations, if a right $\Delta W_6[\mathbb{U}]$ is in the domain, then it will output. If all the $\Delta W_6[\mathbb{U}]$ are wrong, then a random $\Delta W_6[\mathbb{U}]$ will output. */
- 6 Run Line 1 to Line 7 of Algorithm 6 to get (X_1, X'_1) , then compute the message pair (M, M') with (K, K')
- 7 **if** (M, K) 's digest collides with (M', K') 's **then**
- 8 | return $|\Delta C_6[\mathbb{U}]\rangle |y \oplus 1\rangle$
- 9 **else**
- 10 | return $|\Delta C_6[\mathbb{U}]\rangle |y\rangle$

7 Conclusion

By taking the degrees of freedom of the key materials into consideration, we build the automatic tools for the so-called related-key rebound attack, where the degrees of freedom are used to increase the probability of the outbound phase. We develop the new technique to deal with the incompatibilities when searching rebound-attack trails on Saturnin, whose subkeys have very strong relationships. Besides the automatic model, we build new super S-box technique with non-MDS matrix for SKINNY, which is not seen before. For Whirlpool, multiple nested Grover's algorithms are applied to deal with the complex case that both the key schedule path and encryption path adopt rebound attacks. All in all, we achieve certain best free-start collision attacks.

Acknowledgments. This work is supported by National Key R&D Program of China (2018YFA0704701, 2018YFA0704704), the Major Program of Guangdong Basic and Applied Research (2019B030302008), Major Scientific and Technological Innovation Project of Shandong Province, China (2019JZZY010133),

Natural Science Foundation of China (61902207, 61772519, 62072270) and the Chinese Major Program of National Cryptography Development Foundation (MMJJ20180101, MMJJ20180102).

References

1. Zhenzhen Bao, Jian Guo, Danping Shi, and Yi Tu. MITM meets guess-and-determine: Further improved preimage attacks against AES-like hashing. *IACR Cryptol. ePrint Arch.*, 2021:575, 2021.
2. Paulo S.L.M. Barreto and Vincent Rijmen. The WHIRLPOOL hashing function. *Submitted to NESSIE*, 2000.
3. Christof Beierle, Jérémy Jean, Stefan Kölbl, Gregor Leander, Amir Moradi, Thomas Peyrin, Yu Sasaki, Pascal Sasdrich, and Siang Meng Sim. The SKINNY family of block ciphers and its low-latency variant MANTIS. In *CRYPTO 2016, Proceedings, Part II*, pages 123–153. Springer, 2016.
4. Daniel J. Bernstein. Cost analysis of hash collisions: Will quantum computers make SHARCS obsolete. *SHARCS 2009 9: 105*.
5. Alex Biryukov and Ivica Nikolic. Automatic search for related-key differential characteristics in byte-oriented block ciphers: Application to AES, Camellia, Khazad and others. In Henri Gilbert, editor, *EUROCRYPT 2010*, volume 6110, pages 322–344. Springer, 2010.
6. Xavier Bonnetain, Akinori Hosoyamada, María Naya-Plasencia, Yu Sasaki, and André Schrottenloher. Quantum attacks without superposition queries: The offline Simon’s algorithm. In *ASIACRYPT 2019, Kobe, Japan, December 8-12, 2019, Proceedings, Part I*, pages 552–583, 2019.
7. Xavier Bonnetain, María Naya-Plasencia, and André Schrottenloher. Quantum security analysis of AES. *IACR Trans. Symmetric Cryptol.*, 2019(2):55–93, 2019.
8. Gilles Brassard, Peter Høyer, and Alain Tapp. Quantum cryptanalysis of hash and claw-free functions. In *LATIN ’98, Campinas, Brazil, April, 20-24, 1998, Proceedings*, pages 163–169, 1998.
9. Anne Canteaut, Sébastien Duval, Gaëtan Leurent, María Naya-Plasencia, Léo Perrin, Thomas Pornin, and André Schrottenloher. Saturnin: a suite of lightweight symmetric algorithms for post-quantum security. *IACR Trans. Symmetric Cryptol.*, 2020(S1):160–207, 2020.
10. André Chailloux, María Naya-Plasencia, and André Schrottenloher. An efficient quantum collision search algorithm and implications on symmetric cryptography. In *ASIACRYPT 2017, Hong Kong, China, December 3-7, 2017, Proceedings, Part II*, pages 211–240, 2017.
11. Amit Kumar Chauhan, Abhishek Kumar, and Somitra Kumar Sanadhya. Quantum free-start collision attacks on double block length hashing with round-reduced AES-256. *IACR Trans. Symmetric Cryptol.*, 2021(1):316–336, 2021.
12. Carlos Cid, Tao Huang, Thomas Peyrin, Yu Sasaki, and Ling Song. A security analysis of Deoxys and its internal tweakable block ciphers. *IACR Trans. Symmetric Cryptol.*, 2017(3):73–107, 2017.
13. Ivan Damgård. A design principle for hash functions. In Gilles Brassard, editor, *CRYPTO ’89*, volume 435, pages 416–427.
14. Patrick Derbez and Pierre-Alain Fouque. Automatic search of meet-in-the-middle and impossible differential attacks. In Matthew Robshaw and Jonathan Katz, editors, *CRYPTO 2016, Part II*, volume 9815, pages 157–184.

15. Patrick Derbez, Pierre-Alain Fouque, and Jérémy Jean. Improved key recovery attacks on reduced-round AES in the single-key setting. In Thomas Johansson and Phong Q. Nguyen, editors, *EUROCRYPT 2013*, volume 7881, pages 371–387.
16. Patrick Derbez, Paul Huynh, Virginie Lallemand, María Naya-Plasencia, Léo Perrin, and André Schrottenloher. Cryptanalysis results on Spook - bringing full-round Shadow-512 to the light. In Daniele Micciancio and Thomas Ristenpart, editors, *CRYPTO 2020, Part III*, volume 12172, pages 359–388. Springer.
17. Xiaoyang Dong, Jialiang Hua, Siwei Sun, Zheng Li, Xiaoyun Wang, and Lei Hu. Meet-in-the-middle attacks revisited: Key-recovery, collision, and preimage attacks. In *CRYPTO 2021, Proceedings, Part III*, volume 12827, pages 278–308.
18. Xiaoyang Dong, Siwei Sun, Danping Shi, Fei Gao, Xiaoyun Wang, and Lei Hu. Quantum collision attacks on AES-like hashing with low quantum random access memories. In Shiho Moriai and Huaxiong Wang, editors, *ASIACRYPT 2020 Part II*, volume 12492, pages 727–757.
19. Xiaoyang Dong, Zhiyu Zhang, Siwei Sun, Congming Wei, Xiaoyun Wang, and Lei Hu. Automatic classical and quantum rebound attacks on AES-like hashing by exploiting related-key differentials. Cryptology ePrint Archive, Report 2021/1119.
20. Pierre-Alain Fouque, Jérémy Jean, and Thomas Peyrin. Structural evaluation of AES and chosen-key distinguisher of 9-round AES-128. In Ran Canetti and Juan A. Garay, editors, *CRYPTO 2013, Part I*, volume 8042, pages 183–203. Springer.
21. Henri Gilbert and Thomas Peyrin. Super-Sbox cryptanalysis: Improved attacks for AES-like permutations. In *FSE 2010*, pages 365–383, 2010.
22. Vittorio Giovannetti, Seth Lloyd, and Lorenzo Maccone. Architectures for a quantum random access memory. *Physical Review A*, 78(5):052310, 2008.
23. Vittorio Giovannetti, Seth Lloyd, and Lorenzo Maccone. Quantum random access memory. *Physical review letters*, 100(16):160501, 2008.
24. Lorenzo Grassi, María Naya-Plasencia, and André Schrottenloher. Quantum algorithms for the k -xor problem. In *ASIACRYPT 2018*, pages 527–559, 2018.
25. Lov K. Grover. A fast quantum mechanical algorithm for database search. In *Proceedings of the Twenty-Eighth Annual ACM Symposium on the Theory of Computing, Philadelphia, Pennsylvania, USA, May 22-24, 1996*, pages 212–219, 1996.
26. Akinori Hosoyamada and Yu Sasaki. Finding hash collisions with quantum computers by using differential trails with smaller probability than birthday bound. In Anne Canteaut and Yuval Ishai, editors, *EUROCRYPT 2020, Part II*, volume 12106, pages 249–279. Springer.
27. Akinori Hosoyamada and Yu Sasaki. Quantum collision attacks on reduced SHA-256 and SHA-512. In *CRYPTO 2021*, volume 12825, pages 616–646. Springer.
28. Akinori Hosoyamada and Yu Sasaki. Cryptanalysis against symmetric-key schemes with online classical queries and offline quantum computations. In *CT-RSA 2018, San Francisco, CA, USA, April 16-20, 2018, Proceedings*, pages 198–218, 2018.
29. Akinori Hosoyamada and Yu Sasaki. Quantum Demirci-Selçuk Meet-in-the-Middle Attacks: Applications to 6-Round Generic Feistel Constructions. In *SCN 2018*, pages 386–403, 2018.
30. Jérémy Jean, María Naya-Plasencia, and Thomas Peyrin. Improved rebound attack on the finalist Grøstl. In *FSE 2012*, pages 110–126, 2012.
31. Jérémy Jean, María Naya-Plasencia, and Thomas Peyrin. Multiple limited-birthday distinguishers and applications. In *SAC 2013*, pages 533–550, 2013.
32. Jérémy Jean, María Naya-Plasencia, and Martin Schläffer. Improved analysis of ECHO-256. In *SAC*, pages 19–36, 2011.
33. Jérémy Jean, Ivica Nikolić, Thomas Peyrin, and Yannick Seurin. Submission to CAESAR : Deoxys v1.41, October 2016.

34. Marc Kaplan, Gaëtan Leurent, Anthony Leverrier, and María Naya-Plasencia. Breaking symmetric cryptosystems using quantum period finding. In *CRYPTO 2016, Santa Barbara, CA, USA, August 14-18, 2016, Proceedings, Part II*, pages 207–237, 2016.
35. Marc Kaplan, Gaëtan Leurent, Anthony Leverrier, and María Naya-Plasencia. Quantum differential and linear cryptanalysis. *IACR Trans. Symmetric Cryptol.*, 2016(1):71–94, 2016.
36. Hidenori Kuwakado and Masakatu Morii. Quantum distinguisher between the 3-round Feistel cipher and the random permutation. In *ISIT 2010, June 13-18, 2010, Austin, Texas, USA, Proceedings*, pages 2682–2685, 2010.
37. Hidenori Kuwakado and Masakatu Morii. Security on the quantum-type Even-Mansour cipher. In *ISITA 2012, Honolulu, HI, USA, October 28-31, 2012*, pages 312–316, 2012.
38. Mario Lamberger, Florian Mendel, Christian Rechberger, Vincent Rijmen, and Martin Schl  ffer. Rebound distinguishers: Results on the full Whirlpool compression function. In *ASIACRYPT 2009*, pages 126–143.
39. Florian Mendel, Christian Rechberger, Martin Schl  ffer, and S  ren S. Thomsen. The rebound attack: Cryptanalysis of reduced Whirlpool and Gr  stl. In *FSE 2009*, pages 260–276.
40. Florian Mendel, Vincent Rijmen, and Martin Schl  ffer. Collision attack on 5 rounds of Gr  stl. In *FSE 2014*, pages 509–521, 2014.
41. Ralph C. Merkle. One way hash functions and DES. In Gilles Brassard, editor, *CRYPTO '89*, volume 435, pages 428–446.
42. Nicky Mouha, Qingju Wang, Dawu Gu, and Bart Preneel. Differential and linear cryptanalysis using mixed-integer linear programming. In Chuankun Wu, Moti Yung, and Dongdai Lin, editors, *Inscrypt 2011*, volume 7537, pages 57–76, 2011.
43. Mar  a Naya-Plasencia. How to improve rebound attacks. In *CRYPTO 2011*, pages 188–205, 2011.
44. Mar  a Naya-Plasencia and Andr   Schrottenloher. Optimal merging in quantum k-xor and k-xor-sum algorithms. In Anne Canteaut and Yuval Ishai, editors, *EUROCRYPT 2020, Part II*, volume 12106, pages 311–340. Springer.
45. Boyu Ni, Xiaoyang Dong, Keting Jia, and Qidi You. (quantum) collision attacks on reduced simpira v2. *IACR Trans. Symmetric Cryptol.*, 2021(2):222–248, 2021.
46. Bart Preneel, Ren   Govaerts, and Joos Vandewalle. Hash functions based on block ciphers: A synthetic approach. In Douglas R. Stinson, editor, *CRYPTO '93*, volume 773, pages 368–378.
47. Yu Sasaki. Meet-in-the-middle preimage attacks on AES hashing modes and an application to Whirlpool. In *FSE 2011*, pages 378–396, 2011.
48. Yu Sasaki, Yang Li, Lei Wang, Kazuo Sakiyama, and Kazuo Ohta. Non-full-active Super-Sbox analysis: Applications to ECHO and Gr  stl. In *ASIACRYPT 2010*, pages 38–55, 2010.
49. Yu Sasaki, Lei Wang, Shuang Wu, and Wenling Wu. Investigating fundamental security requirements on Whirlpool: Improved preimage and collision attacks. In Xiaoyun Wang and Kazuo Sako, editors, *ASIACRYPT 2012*, volume 7658, pages 562–579.
50. Paul C. van Oorschot and Michael J. Wiener. Parallel collision search with cryptanalytic applications. *J. Cryptol.*, 12(1):1–28, 1999.